

Description and phylogenetic relationships of a large-bodied sphagesaurid notosuchian from the Upper Cretaceous Adamantina Formation, Bauru Group, São Paulo, southeastern Brazil

Galuber Oliveira Cunha^a, Rodrigo Miloni Santucci^{d,*}, Marco Brandalise de Andrade^b, Carlos Eduardo Maia de Oliveira^c

^a University of Brasília, Brazil

^b Pontifícia Universidade Católica do Rio Grande do Sul, Brazil

^c Federal Institute of Education, Science and Technology of São Paulo, Votuporanga, Brazil

^d University of Brasília, Campus Planaltina, Área Universitária n.1, Vila Nossa Senhora de Fátima, Brazil

ARTICLE INFO

Article history:

Received 16 February 2019

Received in revised form

9 August 2019

Accepted in revised form 16 September

2019

Available online 20 September 2019

Keywords:

Sphagesauridae

Cretaceous

Bauru group

Adamantina formation

Osteoderms

Appendicular skeleton

ABSTRACT

In this work we describe new remains and possible gastroliths of a sphagesaurid (Mesoeucrocodylia: Notosuchia) unearthed from the Adamantina Formation (Bauru Group, Upper Cretaceous) in the municipality of Fernandópolis-SP, which add new data about the dental, dermal shield, and the post-cranial skeleton morphology of these crocodylians. Phylogenetic analyses place the studied fossil within Sphagesauridae, in a polytomy with *Armadillosuchus arrudai* and *Caryonosuchus pricei*. The anatomical comparisons are congruent to the phylogenetic analysis since they also suggest that the specimen herein described is closely related to other larger-bodied Sphagesauridae species, such as *Armadillosuchus arrudai*. The new skull, appendicular, and dermal elements described in this work may provide data for the elaboration of new phylogenetic characters which can improve cladistic analyses concerning Sphagesauridae species, as well as they may help to better understand the morphological complexity of this family of crocodylomorphs, especially the large-bodied species.

© 2019 Elsevier Ltd. All rights reserved.

1. Introduction

The Sphagesauridae is one of the most diverse group of Notosuchia and is currently known only to South American Upper Cretaceous deposits, with nine described species to date: *Sphagesaurus huenei*, *Adamantinasuchus navae*, *Armadillosuchus arrudai*, *Yacarerani boliviensis*, *Caipirasuchus montealtensis*, *C. paulistanus*, *C. stenognathus*, *C. mineirus*, and *Caryonosuchus pricei* (Nobre & Carvalho, 2006; Andrade & Bertini, 2008; Marinho & Carvalho, 2009; Novas et al., 2009; Iori & Carvalho, 2011; Kellner et al., 2011; Pol et al., 2014; Leardi et al., 2015b; Fiorelli et al., 2016; Iori et al., 2016; Martinelli et al., 2018). All mentioned species, with exception of *Y. boliviensis*, were unearthed from outcrops of the Adamantina Formation, an Upper Cretaceous sedimentary deposit formed under arid and semi-arid climate by alluvial fans, fluvial

systems, and lakes (Fernandes & Coimbra, 2000; Batezelli, 2010). *Yacarerani boliviensis*, on the other hand, was unearthed from deposits of the Cajones Formation in Bolivia, also of Upper Cretaceous age (Novas et al., 2009; Leardi et al., 2015b).

Coupled with their taxonomic diversity, the sphagesaurids are notosuchian crocodylians of peculiar morphology. This family can be divided in two groups: one of large-bodied forms, like *Armadillosuchus*, *Caryonosuchus*, and *Sphagesaurus*, that have almost twice the skull length of the small-bodied forms, such as *Adamantinasuchus*, *Yacarerani*, and *Caipirasuchus* species. Those animals show a unique dentition, with three distinct tooth morphologies (incisiform, caniniform, and molariform) and a complex pattern of dental occlusion, similar to that seen in mammals, suggesting a degree of herbivory which, until present, has not been reported to any other crocodyliform (Pol, 2003; Andrade & Bertini, 2008; Iori & Carvalho, 2018). Besides their specialized dentition, sphagesaurids possess other traits worthy of mention, such as the complex dermal shield covering *Armadillosuchus arrudai*, with

* Corresponding author.

E-mail address: rodrigoms@unb.br (R.M. Santucci).

an immobile shield of sutured dermal plates covering their cervical region and an articulated banded shield covering the dorsal region similar to that seen in armadillos (Xenarthra, Dasypodidae) (Marinho & Carvalho, 2009).

Despite their high taxonomic diversity, the overall morphology of sphagesaurids, specially the large-bodied forms, remains poorly understood, as most fossils correspond to cranial bones, dentition, and isolated teeth, being scarce fossils that preserve well the post-cranial skeleton (Pol et al., 2014; Leardi et al., 2015b; Iori et al., 2016; Martinelli et al., 2018), or reports that explore morphofunctional aspects of these animals beyond their feeding mechanism and feeding ecology (Pol, 2003; Iori & Carvalho, 2018). Hence, the phylogenetic hypothesis of this group is based mainly on characters concerning the cranial and dental morphology (Pol et al., 2014; Leardi et al., 2015b), grouping sphagesaurids in a monophyletic group, with *Adamantinasuchus navae* and *Yacarerani boliviensis* forming a group of basal forms and as a sister clade to a group formed by other two monophyletic groups, one comprised by the species of *Caipirasuchus* and another formed by *Sphagesaurus huenei*, *Armadillosuchus arrudai*, and *Caryonosuchus pricei* that represent large-bodied sphagesaurids.

In this sense, the present work brings the description of new fossils of a large-bodied sphagesaurid from the Adamantina Formation which are assigned as *Armadillosuchus* sp.. It also reports novel data about the elements of the dermal shield, tooth morphology, mandible, and data on the post-cranium skeleton, which until now were mostly known for small-bodied sphagesaurids such as *Yacarerani* and *Caipirasuchus montealtensis* and *C. paulistanus* (Pol et al., 2014; Leardi et al., 2015b; Iori et al., 2016).

2. Geological setting

The Upper Cretaceous Bauru Group (Fig. 1) covers the states of Goiás, Mato Grosso, Mato Grosso do Sul, Minas Gerais, São Paulo, and Paraná, and is predominantly characterized by deposits formed under arid/semi-arid climate conditions (Batezelli, 2010) which, at the same time, comprised water bodies essential for the maintenance of several organisms (Goldberg & Garcia, 2000; Garcia et al., 2005). This group is usually subdivided into four formations, representing different depositional systems that are partially coeval: Araçatuba Formation (lacustrine), Adamantina and Uberaba formations (fluvial), and Formation Marília (alluvial) (Fernandes & Coimbra, 2000; Goldberg & Garcia, 2000). Alternatively, Basili et al. (2016) considered part of this sedimentary sequence as a fluvial distributary system, where the most basal units are considered to be basinal or distal/medial portions of endorheic fluvial systems and the upper units mostly represent palaeosols.

In this context, the Adamantina Formation is an important fossiliferous unit with a rich record of vertebrates such as amphibians, lizards, testudines, dinosaurs, and mainly crocodyliforms, which have a large number of fossil species described (Candeiro & Rich, 2010).

The age of the Adamantina Formation is disputed, since Dias-Brito et al. (2001) suggested a Turonian-Santonian age based on records of ostracods and charophytes and, on the other hand, Gobbo-Rodrigues et al. (1999) and Santucci & Bertini (2001) attributed to it a Campanian-Maastrichtian age based on ostracods and vertebrates, respectively. Recently, Castro et al. (2018) performed a radiometric dating using zircon crystals and found that the Adamantina Formation deposits from the region of General Salgado are 87.8 Ma old, which suggests that the deposition of the

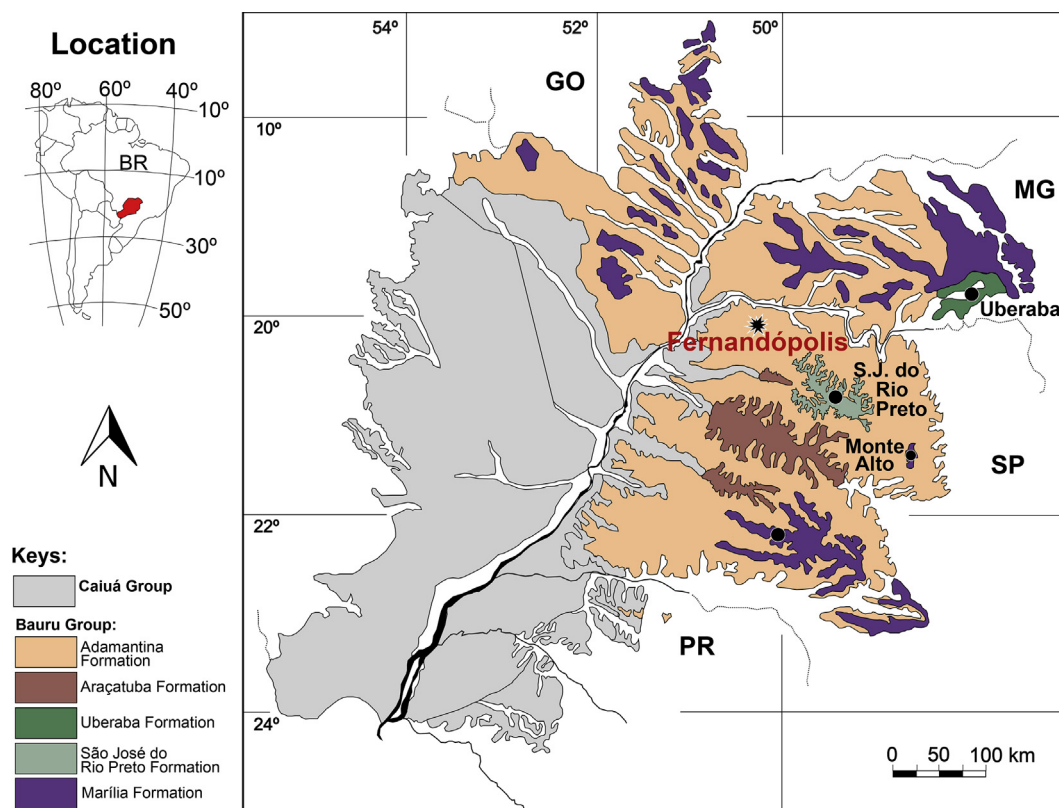


Fig. 1. Geological map of the Bauru Group highlighting the area where the sphagesaurid material has been found (Adamantina Formation). Map compiled from Fernandes (1998) and Fernandes & Coimbra (1996). GO, MG, SP, and PR: Goiás, Minas Gerais, São Paulo, and Paraná states, respectively.

unit occurred at least between the Coniacian and the Maastrichtian. Magnetostratigraphic data provided by Tamrat et al. (2002) for the Uberaba and Marília formations indicate that these units are younger than the Cretaceous normal polarity quiet zone (~121–83 Ma; see Granot et al., 2012), which means that they cannot be older than the Santonian/Campanian interval. The Adamantina Formation not only is reported as coeval to the Uberaba Formation, but it has, in some instances, a gradational contact with the overlying Campanian/Maastrichtian Marília Formation (Batezelli et al., 2003; Batezelli, 2017). Thus, in the light of most of evidence reported so far, we consider the Adamantina Formation as Campanian-Maastrichtian in age.

The fossil described in this paper was collected in the municipality of Fernandópolis, São Paulo State. Two main outcrops, approximately 150 m apart from each other, have been found in this locality. The outcrop 1 has the best exposures and complements the description of the sequence seen in the outcrop 2, from which the study material was collected.

The base of the outcrop 1 comprises very fine to fine, massive, reddish/brown, sandstone, with millimetric to submillimetric carbonate pebbles. Toward the top, portions of the same type of sandstone are found, but with fine to medium granulation and with a higher concentration of carbonate pebbles. This portion is approximately 4 m thick. From this level, a crocodylomorph egg with associated eggshells was found. There are invertebrate ichnofossils in the contact between this portion and an overlying bed which is, at least, 5.4 m thick, comprising essentially fine to medium sandstone interbedded with reddish silty sandstone. Very few ichnofossils are observed. This sequence is similar to the contact between the Jales Lithofacies (see Batezelli, 2010) and the other deposits of the Adamantina Formation.

The outcrop 2, from which the study material was collected, presents the same fine to very fine sandstone described for the Jales Lithofacies (see Batezelli, 2010) and is approximately 2 m thick. At the top, dermal plates and bone fragments of Baurusuchidae were found.

In this same outcrop an almost complete juvenile Baurusuchidae (lacking the caudal vertebrae), an isolated egg, a partial caudal vertebra of Baurusuchidae, *Skolithos* and *Taenidium*-like ichnofossils were also found.

3. Material and methods

3.1. Material

IFSP-VTP/PALEO-0001 consists of isolated teeth and skull elements, ribs and gastral elements, left and right manus, complete right fore-limb, and several osteoderms. The fossil was found partially articulated and fragmented in the rock, with exception of few complete elements, such as the right fore-limb and the left manus which had most of their elements articulated.

3.2. Descriptive parameters

The following description follows the same anatomical orientation and nomenclatural standards used in the descriptive studies of *Simosuchus clarki* and *Yacarerani boliviensis* (Pol, 2003; Andrade & Bertini, 2008; Georgi & Krause, 2010; Hill, 2010; Kley et al., 2010; Sertich & Groenke, 2010; Pol et al., 2014; Leardi et al., 2015b).

3.3. Compared material

The anatomic comparisons were based on the description of other sphagesaurids and some non-sphagesaurid notosuchians such as *Adamantinasuchus naveae*, *Armadillosuchus arrudai*,

Caipirasuchus paulistanus, *C. montealtensis*, *C. stenognathus*, *Carayonosuchus pricei*, *Sphagesaurus huenei*, *Yacarerani boliviensis*, *Notosuchus terrestris*, *Araripesuchus tsangatsangana*, *Baurusuchus albertoi*, *Montealtosuchus arrudacamposi*, and *Simosuchus clarki* (Pol, 2003; Pol, 2005; Nobre & Carvalho, 2006; Turner, 2006; Tavares, 2007; Andrade & Bertini, 2008; Marinho & Carvalho, 2009; Novas et al., 2009; Georgi & Krause, 2010; Hill, 2010; Kley et al., 2010; Nascimento & Zaher, 2010; Sertich & Groenke, 2010; Iori & Carvalho, 2011; Kellner et al., 2011; Iori et al., 2013; Pol et al., 2014; Tavares et al., 2015; Leardi et al., 2015b; Fiorelli et al., 2016; Iori et al., 2016; Tavares et al., 2017).

3.4. Phylogenetic analysis

The analysis was conducted using the software TNT 1.5 (Goloboff & Santiago, 2016) under equally weighted parsimony. We scored the anatomical information of IFSP-VTP/PALEO-0001 into the dataset of Martinelli et al. (2018). We also changed the state of the character 106 for *Armadillosuchus arrudai* (char. 106-3 to char. 106-2). This character represents the number of premaxillary teeth and undescribed new specimens of *A. arrudai* shows evidence that those animals had three and not only two premaxillary teeth (Marinho pers. comm.), contrary to the diagnosis of the species (Marinho & Carvalho, 2009). This dataset represents the most recent phylogenetic information on sphagesaurids and other notosuchians and it is also an updated version of previous works (Pol et al., 2014; Leardi et al., 2015a; Leardi et al., 2015b; Fiorelli et al., 2016), adding new cranial, mandibular, and postcranial characters and new taxa. The updated data matrix consists of 440 characters and 114 terminals after the insertion of IFSP-VTP/PALEO-0001 (Appendix 1). Neosuchians are summarized in a single terminal. Characters were treated as unordered and equally weighted, without a preferential *a priori* defined optimization method (ACCTRAN/DELTRAN). A heuristic search was conducted with 10,000 random addition sequences, followed by Tree Bisection Reconnection (TBR), saving ten trees per round (random seeds = 1). The resulting cladograms went through a final round of TBR branch swap. A strict consensus was used to summarize the results obtained on each search.

4. Systematic paleontology

CROCODYLORPHA Walker (1970)

CROCODYLIFORMES Hay (1930)

MESOEUCROCODYLIA Whetstone & Whybrow (1983)

NOTOSUCHIA Gasparini (1971)

SPHAGESAURIDAE Kuhn (1968)

ARMADILLOSUCHUS Marinho & Carvalho (2009)

Type species: *Armadillosuchus arrudai* Marinho & Carvalho (2009)

Diagnosis. A sphagesaurid bearing two premaxillary teeth, the second ones are hypertrophied caniniforms; posterior maxillary teeth present the major crown axis obliquely oriented with few large tubercles disposed in one lingual keel; lower jaw is narrow and elongated at the symphyseal region; first dentary teeth facing anteriorly; fourth dentary teeth slightly flattened laterally bearing anterior keels; fifth dentary teeth has the major crown axis obliquely oriented with the tuberculated keel facing the labial margin, and occluded behind the third maxillary teeth; basioccipital-basisphenoid suture surrounds the foramen intertympanicum posteriorly; foramen intertympanicum in the basi-sphenoid; basioccipital-basisphenoid suture surrounds the lateral Eustachian foramina posteriorly and laterally; lateral Eustachian foramina aligned to the foramen intertympanicum; antorbital depression divided into two parts: a smooth and deeper and an

ornamented and shallower one; body armor with two distinct parts: a cervical shield and a banded dorsocervical section; hexagonal osteoderms compose most of the cervical shield (Marinho & Carvalho, 2009).

ARMADILLOSUCHUS sp.

Described specimen. The material is a fragmentary specimen made up from circa of 165 bony elements and fragments, being 95 of these, osteoderms, with many of them being well preserved and representing part of the cranium, mandibles and teeth, axial skeleton, appendicular skeleton, and body armor of a new specimen of a large sphagesaurid. The material is kept at the collection of the Federal Institute of Education, Science and Technology of São Paulo (Votuporanga, São Paulo, Brazil) under the catalog number IFSP-VTP/PALEO-0001.

Locality and horizon. Rural area of the municipality of Fernandópolis-SP, Brazil, in outcrops of the Adamantina Formation, Upper Cretaceous (Campanian-Maastrichtian) of the Bauru Basin.

Description

The described fossil was partially exposed in the soil at the outcrop area, because of that some of the elements have a brown color and are more fragile and fragmented, while the others are white in color and were found in a less weathered sandstone, thus these elements present a better preservation. Most of the elements were partially articulated in the rock, such as the ribs, elements of the left *carpus* and *manus*. The described material is considered to represent only one individual because there are no repeated elements and some teeth and ribs present both types of preservation mentioned above.

Teeth

Most teeth associated to the specimen are isolated and nine of them are relatively well preserved. There is also preserved a maxillary replacement tooth and other two pre-maxillary alveoli containing parts of a hypertrophied caniniform and an unidentified tooth. Because of the nature of most teeth (isolated), their description only identifies them as incisiforms, caniniforms, and molariforms, based on their morphology, and do not attempt to provide information on their orientation or alveolar correspondence.

Incisiforms (Fig. 2A1). Only one tooth was identified as an incisiform and it is not possible to determinate whether it is a premaxillary or mandibular tooth. It is an isolated tooth that can be distinguished from caniniform and molariform teeth by its smaller size and more rounded cross-section. The tooth is 9 mm tall, has only part of the crown preserved and shows a distinctive wear facet at the apical portion. The crown base has a slightly elliptical cross-section with approximate dimensions of 7.5 × 8.5 mm. In general, the tooth is conical and is ornamented with vertical crests; most of these crests extend from the base to the apex of the crown, while others end at the first half of the crown and some at the second half, but not reach the apex of the crown. The spacing between crests is irregular and in the surface where the wearing is evident, those crests are more spaced than those at the opposite side of the crown. The enamel coating of the crown has a rugose texture with micro-crests and pebbles.

Caniniforms (Fig. 2A2). One caniniform tooth is well preserved, comprising the entire crown and part of its root. The tooth is conical and slightly curved distally having crown measures of 15.0 mm of width by 18.6 mm of length at its base and a crown height of 30.0 mm. The crown is ornamented with vertical crests that seem to be less developed than those of the incisiform tooth. Those crests extend from the base to the apex of the crown, with one exception that extends only to its mid height. The spacing between crests at the base averages about 3.0 mm. The enamel has a rugose texture but is less developed than in the other described teeth. There are two visible wear facets, one at the crown apex and another that wears most of what would be the lingual surface of the tooth. This

last wear facet also shows well developed and sub-horizontal striae. The tooth root has vertical parallel sulci and crests, which are intercalated, being around 0.5 mm the spacing between their crests.

Molariforms (Fig. 2A3, 2B, 2C). Seven molariform teeth were identified and five of them have portions of their roots preserved. These teeth have a triangular cross section, being conical and slightly curved backwards. A characteristic keel projects obliquely to the sagittal axis of the crown. The teeth dimensions vary, ranging from 10.0 to 12.0 mm in crown base width, from 16.0 to 18.0 mm in crown base length, and from 14.0 to 18.0 mm in height (depending of the wearing state of the tooth apex). These teeth also show basal-apical crests along the crown which are well-developed, being the spacing among them around 2.5 mm. The crests extend from the base of the crown up to the crown mid portion. The enamel has the rugose texture, with well-developed micro-crests and pebbles. Sub-horizontal striae are also present in wear facets and vary in intensity depending on the tooth observed. The keel on these teeth are robust, except for the keels that are clearly worn, with denticles (serrations) of different dimensions – better observed in the maxillary replacement tooth that has not been worn – with those of the basal and apical portion of the keel being smaller than those at the mid portion. This keel (also seen in the replacement maxillary molariform tooth) present a pattern of paired-denticles (Fig. 2C) where each pair is divided by an interdenticle sulci while within the pair the denticles are divided by a shallower sulcus (Fig. 2C2 and 2C4). In the teeth with preserved roots there is a constriction (cingulum) delimitating the root and crown portions. This constriction does not form a horizontal boundary, instead the border between root and crown forms a sinuous contact. The molariform roots also present the same pattern of intercalated micro-crest and sulci already described for the caniniform.

Cranium

Premaxilla (Fig. 3A). A right fragment of premaxilla in direct contact with the maxilla is preserved. In anterior view it is possible to identify the lateral convexity of the premaxilla with the inferior portion representing the lateral surface and the ventral edge of the rostrum, while the superior portion is slightly convex and represents the transition between the lateral and dorsal surface. Those two portions are well distinguishable by their different ornamentation pattern. Furthermore, in anterior view, it is possible to see that at least some part of the wall of the caniniform alveolus, which is hypertrophied in comparison to the other alveoli, is made up by the anterior surface of the pre-maxilla. Due to the fragmentary nature of these elements, the dorsal view brings only information on the lateral convexity of this portion of the snout, information on the ornamentation, which is better described in lateral view and, mainly, it brings information on the caniniform alveolus. This alveolus is not fully preserved, but still represents most of the dorsal view of the pre-maxilla, as it extends 31.5 mm dorsally and distally overlapping the last premaxillary alveolus and almost reaching the contact premaxilla-maxilla. In ventral view, it is possible to see the mesial surface of the premaxilla forming the alveolar wall of the caniniform tooth and the last premaxillary tooth, which contain fragments of what is probably their respective replacement teeth. The alveolar distal wall of the last premaxillary tooth is formed entirely by the premaxilla, which invaginates distally at the suture point with the maxilla. In lateral view this fragment is well-preserved, and it is possible to see the premaxilla-maxilla suture extending vertically and the continuity of the ventral edge of the premaxilla, which limits the alveolar walls laterally. Also, in lateral view, it is worth to mention the size of the premaxilla-maxilla neurovascular foramen, which present a diameter of approximately 6.65 mm while the longest length

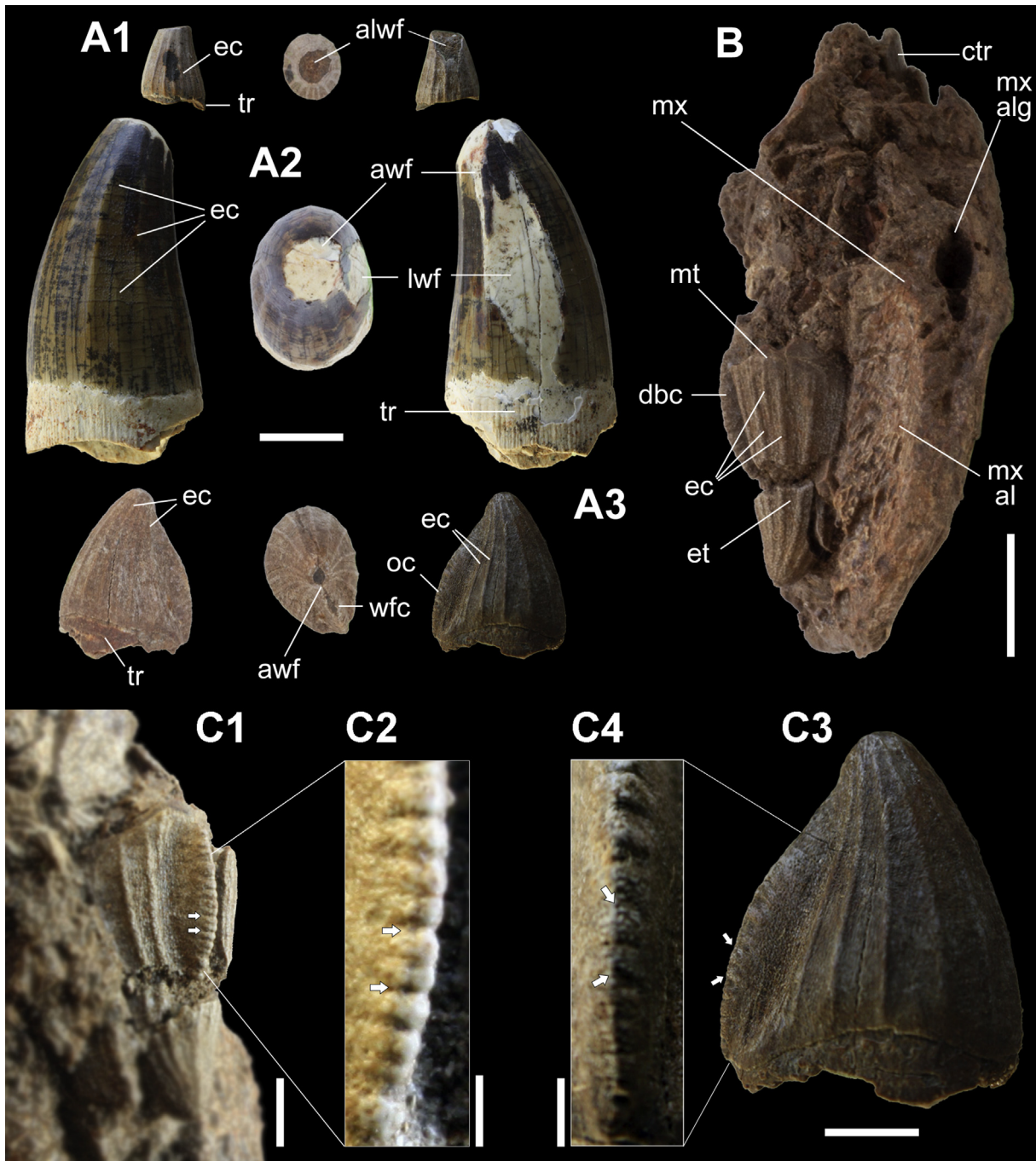


Fig. 2. Tooth morphology of *Armadillosuchus* sp. **A:** the three different tooth morphologies found: incisiform (A1), caniniform (A2), and molariform (A3) in labial, apical, and lingual views. **B:** right maxilla in posterior view with a replacement molariform tooth preserved and a partially preserved maxillary alveolus. **C:** molariform teeth in lateral view with preserved serrations both in a replacement tooth (C1) and in an isolated tooth (C3); detail of the serrations (C2 and C4), arrows indicate the pattern of double-denticles. **Abbreviations:** *alwf* = apical-lateral wear facet; *awf* = apical wear facet; *ctr* = caniniform tooth root; *dbc* = distal-buccal carina; *ec* = enamel crests; *et* = enamel rugose texture; *lwf* = lateral wear facet; *mt* = molariform tooth; *mx* = maxilla; *mx alg* = maxillary alveolar groove; *mx al* = maxillary alveolus; *oc* = oblique carina; *tr* = tooth root; *wfc* = wear facet on the carina. **Scale bars:** A-B, C1 and C3 = 1 cm, C2 and C4 = 0.1 cm.

measures 48 mm, more than 10% of the preserved portion of the premaxilla and clearly longer than the other preserved foramina. The superior portion of the premaxilla is ornamented by sulci, pits, and keels, while the inferior portion has a smooth surface being ornamented only by the premaxilla-maxilla foramen. In medial view, it is possible to see the extension of the caniniform alveolus and how it extends and curves dorsally on top of the last premaxillary alveolus.

Maxilla (Figs. 2B, 3A-B). Two fragments of the right maxilla are preserved. One comprises the anteriormost portion of the bone, in direct contact with the premaxilla, and the another corresponds to the posterior portion of the element, in contact with the lacrimal and jugal.

Fragment 1 (Figs. 2B and 3A) is in contact with the right premaxilla forming one of the preserved portions of the rostrum present in IFSP-VTP/PALEO-0001. As in the premaxilla, most of the

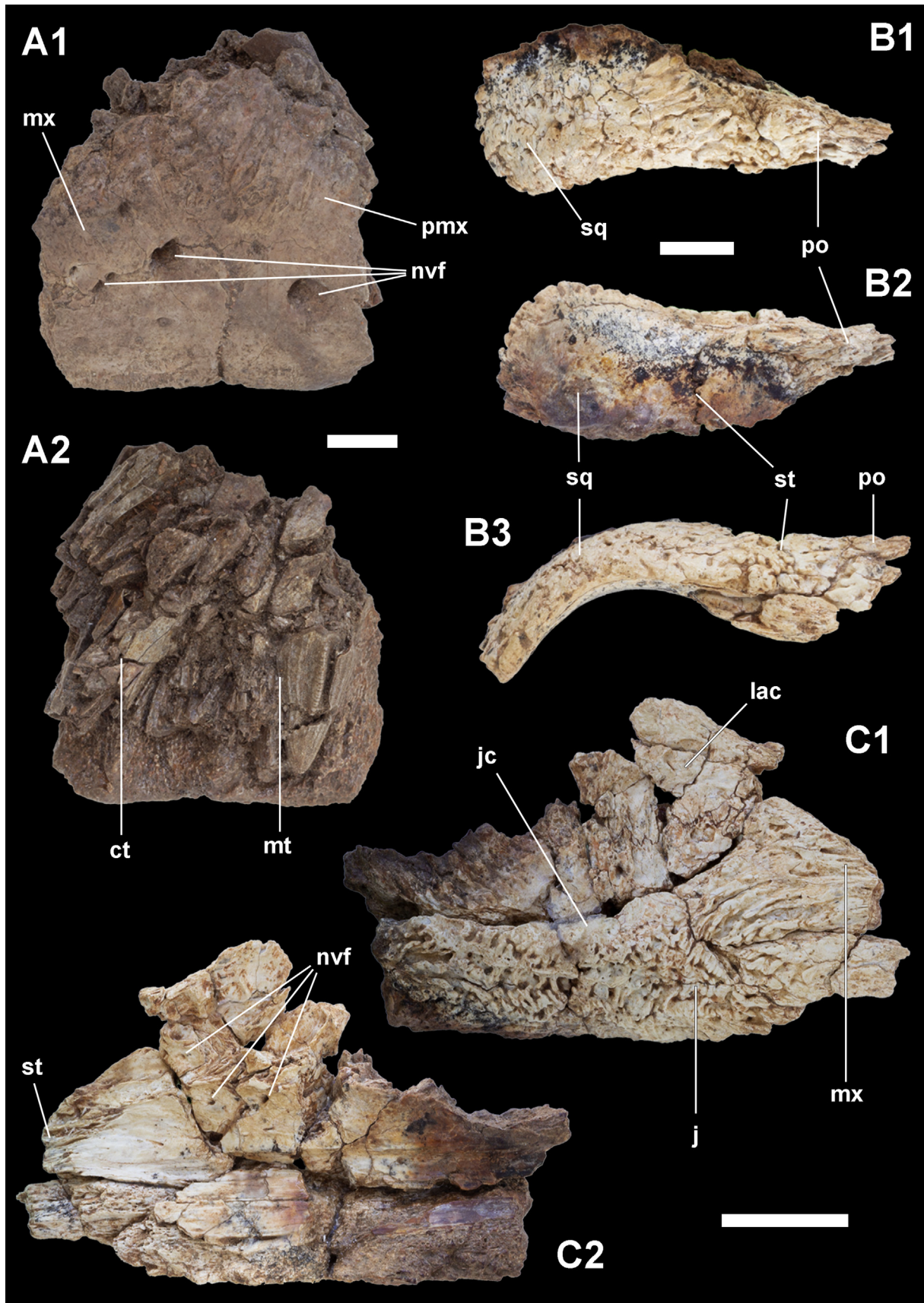


Fig. 3. Preserved elements of the cranium. **A:** Right premaxilla and maxilla in lateral (A1) and medial (A2) views. **B:** Right postorbital and squamosal in dorsal (B1), ventral (B2) and lateral (B3) views. **C:** Right maxilla, lacrimal and jugal in lateral (C1) and medial (C2) views. **Abbreviations:** *ct* = caniniform tooth; *j* = jugal; *jc* = jugal crest; *lac* = lacrimal; *mt* = molariform tooth; *mx* = maxilla; *nvf* = neurovascular foramina; *pmx* = premaxilla; *po* = postorbital; *sq* = squamosal; *st* = suture. **Scale bars:** A-B = 1 cm; C = 2 cm.

information available in dorsal view of this fragment concern the lateral convexity of this portion of the rostrum. The lateral convexity of the maxilla is less pronounced than that described for the premaxilla. This difference may be noticed by a slight step between the two elements in dorsal and posterior views. The ornamentation pattern of the maxilla, in lateral view, is similar to the condition observed in the premaxilla: restricted to the superior portion of the element and, as for the inferior portion, this is smooth with small neurovascular foramina, except for one foramen posterior to the premaxilla-maxilla suture. The first maxillary alveolus contains a replacement molariform tooth well preserved and, as for the second alveolus, only part of its proximal alveolar wall is preserved. Also, in posterior view, it is possible to see a large elliptical opening/channel connecting the neurovascular foramina in the lateral view of the element.

Fragment 2 (Fig. 3B) is in contact with the lacrimal and the jugal. This fragment consists only in a small portion of the maxilla representing the suture between those three bones. The ornamentation pattern present in this fragment is similar to that seen in the other fragment previously described.

Lacrimal (Fig. 3B). The right element is preserved and comprises a small fragment representing the pre-orbital region in contact with the maxilla and jugal. Except for the lateral view, the features present in the fragment cannot be evaluated due to its poor preservation state. The mesial surface is also not fully preserved and exposes the layers forming the bone structure at the maxilla-lacrimal suture. In lateral view, the maxilla-lacrimal suture extends vertically along the anterior portion of the fragment, while the lacrimal-jugal suture extends horizontally along the ventral portion of the fragment. This surface is ornamented by sulci, grooves, and pits like that observed in the premaxilla and maxilla.

Jugal (Fig. 3B). The right jugal fragment is preserved and represents the infraorbital region in contact with the maxilla and lacrimal. The anterior and posterior views provide information on the width of the preserved fragment and its lateral convexity, with its most convex portion forming a crest that extends longitudinally and separates the lateral surface in two portions. The superior portion of the jugal is dorsally limited by the jugal-lacrimal suture, as for the inferior portion, which is more medially curved. The whole fragment is ornamented by sulci, grooves, and pits, and this ornamentation intensifies towards the jugal crest at the inferior portion. In medial view, the fragment is more complete than the lacrimal and the maxilla in the same bone element, which allows to identify neurovascular foramina close to the sutures. The jugal does not present the ornamentation described for the lateral surface.

Post-orbital and squamosal (Fig. 3C). A single fragment representing the right post-orbital region comprising the suture between post-orbital and squamosal. The suture is observed in all views and forms an oblique contact between these bones. The fragment has the same ornamentation pattern (with sulci, grooves, crests, and pits) except by its ventral surface, which is completely smooth. The squamosal fragment is posteriorly curved, consisting in the lateral and posterior limits of the cranium roof.

Dentary (Fig. 4A-B). Two elements are preserved representing fragments of both right and left mandibles.

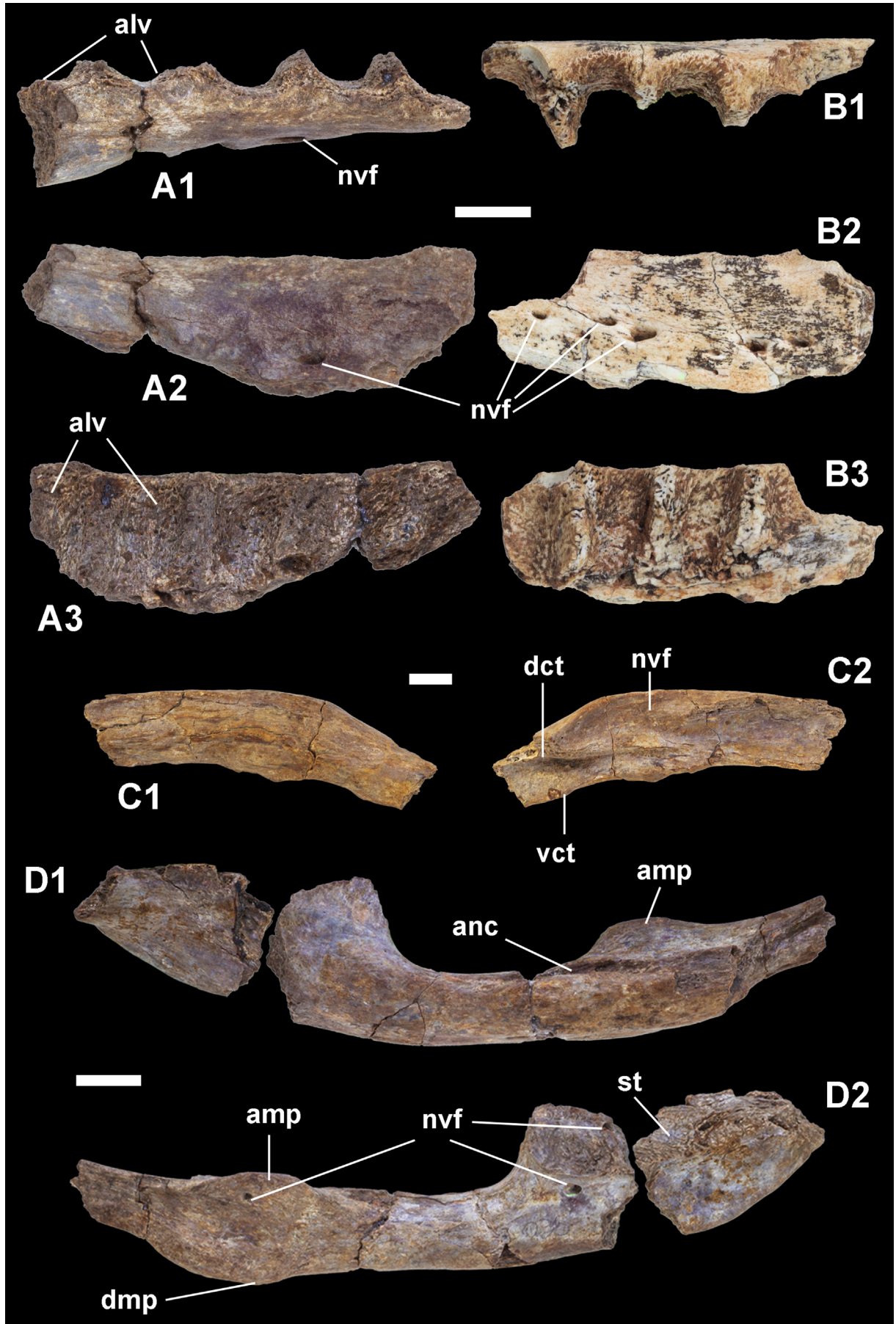
Fragment 1, left side, anterior portion (Fig. 4A) – this fragment preserves part of the dorsal and lateral surfaces of the mandibular symphysis and part of four alveoli. There are differences in the structure of the alveoli which are best seen dorsal view; the anteriormost alveolus is the least complete, but it is possible to observe a medial displacement compared to the others. The following two alveoli seem to have their proximal and distal walls

perpendicularly aligned to the longitudinal axis of the fragment. As for the last alveolus, its proximal portion is longitudinally oblique, with its medial portion displaced anteriorly. In the lateral surface there are nine neurovascular rounded/elliptical foramina of approximately the same size. Some of the foramina are also seen in dorsal and medial views, opening in a groove that runs ventrally to the alveoli. The fragment does not present any ornamentation except by the foramina and that typical of the alveolar walls, with sulci.

Fragment 2, right side, posterior portion (Fig. 4B) – this fragment preserves portions of the lateral and dorsal surface of the mandible and parts of five dentary alveoli. A posterior-lateral projection can be observed in dorsal view, which is not followed by the alveolar line, making the posterior portion of the fragment expanded when compared to the rest of the fragment. The first and last alveolus preserved are the least complete, but it seems that there is a gradual reduction in the alveoli dimension towards the posterior alveoli. This fragment is also smooth, with no ornamentation, except for the alveolar walls and one foramen at the posterior portion at the lateral surface of the fragment.

Surangular (Fig. 4C). The right surangular preserves part of the anterior and posterior mandibular rami that make up the dorsal margin of the mandibular fenestrae. The anterior ramus is more robust than the posterior one and is ventrally curved, while the posterior ramus is thinner and has no apparent curvature. The element is mostly smooth, without the typical ornamentation described for the cranium, but presenting some rugose portions at the dorsal surface. The dorsal tuberosity of the coronoid is partially observed in medial view and the ventral tuberosity of the coronoid, which is not as well as developed as the latter, is fully observed in the same view. Posteriorly to the ventral tuberosity of the coronoid, on the ventral surface, there is a rugose depression, probably indicating a muscular insertion scar. Between the dorsal and ventral tuberosity there is a horizontal sulcus, which is interpreted as the region for accommodation of the *cartilago transiliens*. A depression excavates the medial surface of the posterior ramus, giving the fragment a crescent cross-section.

Angular (Fig. 4D). Two complementary fragments of the right side are preserved. The smaller fragment represents the posterior portion of the mandibular ramus, as for the larger fragment, it represents the ventral margin of the external mandibular fenestra. In lateral view there is a fossa at the ventral margin of the external mandibular fenestra. This fossa is delimited laterally by the crest below the external mandibular fenestra and is aligned with the lateral margin of the angular. At the posterior portion, both the fossa and the crest are less developed until they disappear right before the posterior margin of the external mandibular fenestra. Still in lateral view, it can be observed the development of the medial ascending process of the angular, while in medial view, another process develops ventrally to the former. Between these processes there is a shallow depression of rugose texture, indicating a probably muscular insertion area. This depression ends posteriorly alongside the posterior limits of the mentioned processes and, anteriorly, this depression is interrupted by the fragmentation of the element. Three neurovascular foramina are visible on the fragment: two in medial view, being one below the apex of the medial ascending process and another one located more posteriorly, at the anterior portion of the ventral limit of the surangular-angular suture; the third foramen can be seen at the lateral surface of the base of the medial ascending process of the angular. Finally, is worth of note a depression located at the anterior portion of the ventral surface, which is interrupted by the fragment fracture and is medially delimited by the ventral portion of the medial process.



Axial skeleton

Vertebra (Fig. 5A). Fragmentary vertebral centrum with no determined position or orientation, but still, it preserves one of its articulation facets, which is slightly concave. The fragment is robust with a slight lateral compression, resembling the centrum of a trunk vertebrae.

Cervical rib (Fig. 5B). One right cervical rib is partially preserved, lacking parts of the anterior and posterior processes. The extension of those processes forms the articulation facets with the adjacent (anterior and posterior) cervical ribs of the series, being evident the area for accommodation of the next rib in latero-ventral view.

Thoracic ribs (Fig. 5C-D). Six fragments are preserved, from which it is possible to identify the approximate position in the thoracic series and to which part of the rib is preserved. Three of these ribs preserve the proximal portion, being possible to observe the base of the *capitulum* and *tuberculum*, corresponding the anterior ribs, while the other three ribs preserve their distal portions and seem to represent posterior ribs. In general, the dorsal lateral surface is flatter than the ventral medial portion, and, when observed in lateral view, the preserved fragments are straight.

On the ribs considered to be anterior, the neck region (the portion immediately before the bifurcation between the *capitulum* and *tuberculum*) is constricted and have a rounder cross-section when compared to the diaphysis cross-section, which in turn, is broader and flattened. The *tuberculum* base projects anteriorly and medially, while the *capitulum* seems to be projected medially and in a straight manner. The most anterior of these ribs present part of the proximal region of its diaphysis preserved. In the anterior portion of this region an anterior keel is present, which is only observed in this rib.

The posterior ribs were unearthed in close association, aligned side by side, possibly representing consecutive elements of the thoracic rib series. Two of these ribs preserve part of its distal end and present at this region a rugose texture. Additionally, these ribs seem to be larger and have larger distal widths when compared to the anterior ribs described above. The most posterior of these ribs have a rounder cross section in comparison to the other two posterior ribs.

Gastralia (Fig. 5E). Isolated fragments and articulated portions of the elements of the gastralia are preserved. Some of these fragments are considered to represent the distal portion of these bones, as they have a flat end, like a blade. The isolated fragments, in general, have an elliptical cross section. Some fragments were found articulated and were kept in the sedimentary matrix. They seem to be broader but have a more elliptical cross section.

Appendicular skeleton

Coracoid. A fragment of the left coracoid preserving the coracoid foramen is preserved. The lateral opening of the foramen is displaced anteriorly and is more elliptical than the medial opening.

Humerus (Fig. 6). A nearly complete right humerus was found fragmented during the preparation process, with elements of the diaphysis and epiphysis separated, but close to each other, which allowed its reconstitution during preparation. The general measures are: 193 mm of total length, 71 mm of proximal epiphysis width, 72 mm of distal epiphysis, and 23,50 mm of diaphysis width at its mid-point, which has an approximate circular shape. In anterior and posterior views, the element seems to be straight, but its sinuosity is better observed in lateral or medial view.

In anterior view, the proximal portion expands laterally from the mid-point of the diaphysis. This expanded region matches the beginning of the deltoid crest at its distal portion. The proximal surface is straight, forming an angle of approximate 90° with the lateroproximal surface. It is not possible to identify the glenohumeral condyle. The medioproximal surface present a depression that corresponds to the medial humeral process. The deltoid crest is well developed along the lateroproximal surface of the humerus and corresponds to most of the superior portion of the diaphysis, with the crest for insertion of the triceps developing laterally to it at the proximal third of the deltoid crest. The fossa for insertion of the *M. coracobrachialis brevis* is broad but not deep. The articulation surface is well developed but does not extend further the anterior portion of the epiphysis, although it extends up to the posterior region. Right below the articular surface, in posterior view, there is the fossa for insertion of the *M. scapulothoracalis*. This fossa is delimited laterally by a crest on the posterior surface of the humerus, which in turn, separates this fossa from the scar for insertion for the *M. teris major*. The distal epiphysis is anterodorsally flattened and has a well-developed and laterally expanded articular facet, like in the proximal epiphysis, but not as expressive as the latter. The proximal epiphysis does not extend anteriorly. On the other hand, the distal epiphysis does not extend posteriorly, but extends anteriorly until the beginning of the anterior distal humeral depression. This depression is more developed than its opposite part, the posterior distal humeral depression which, in turn, is shallower and broader. The ulnare and radiale supracondylar crests are visible in posterior view, being the former crest more developed than the latter. The distal portion of the humerus, in medial view, has a fossa for accommodation of the *M. flexor digitorum longus* right above the ulnare articular surface of the humerus.

Radius (Fig. 7A-D). The right radius is almost complete, lacking only parts of the distal epiphysis, and the left radius is represented only by part of the diaphysis. The right radius measures approximately 186 mm of length, 36 mm and 33 mm of width at the proximal and distal epiphysis, respectively. The diaphysis is approximately straight and has an oval cross-section with its anteroposterior axis being the major one. The humeral articular surface extends laterally along the proximal epiphysis. The medial crest is smooth and little developed, same as the lateral crest, which is best seen at the lateroposterior portion of the diaphysis.

Ulna (Fig. 7E-H). The right ulna is well preserved, even though it presents many fractures, specially a major crack that, apparently, is responsible for the rotation of the distal portion of the element during the diagenesis. The ulna has approximately 202 mm of total length, being slightly longer than the humerus. The proximal epiphysis has approximately 30 mm of width, but the radio-ulnare-humeral articular facet is broken to fully assess this measure. As for the distal epiphysis, it has approximately 20 mm of width. The diaphysis has an approximate triangular section and curves in a gently manner medially. The ulnare-humeral surface is slightly concave and broad. The radiale facet is not well-developed. Only the basal portion of the olecranon process is preserved, thus, it is not possible to describe its development. The fossa for the *M. pronator quadratus* is well developed in medial view. The anterior crest is well developed with its distal end sharper than the proximal end. The lateral crest develops along the entire lateral surface until the distal and proximal epiphysis. The crack and torsion observed in the distal end of the ulna is better observed in

Fig. 4. Elements of lower jaw. **A:** Posterior portion of the right dentary in dorsal (1), lateral (2) and medial (3) views. **B:** Anterior portion of the left dentary in dorsal (1), lateral (2) and medial views. **C:** Right surangular in lateral (1) and medial (2) views. **D:** Right angular in lateral (1) and medial (2) views. **Abbreviations:** *alv* = alveoli; *amp* = ascending medial process; *anc* = angular crest below external fenestra; *dct* = dorsal coronoid tuberosity of surangular; *dmp* = descending medial process; *mg* = Meckel's groove; *nvf* = neurovascular foramina; *st* = suture; *vct* = ventral coronoid tuberosity. **Scale bars** = 1 cm.

distal view. The posterior oblique process and the anterolateral process are well defined; the former develops as a sharp crest that forms the distal limit of the ulna, while the latter develops as a projection and ends before the distal limit. Between these processes there is a sulcus that extends until the articular surface, making the anterior articular surface concave while seen in lateral view.

Carpus and manus

The elements described for the left *manus* were semi-articulated in the sedimentary rock and separated (Fig. 8) during preparation. The general measures of both *manus* are presented in Table 1.

Radiale (Figs. 8, 9A). The right and left *radiale* are well-preserved, with an average length of 54 mm and 37 mm and 30 mm of width at its proximal and distal portions, respectively. In general, it is anteroposteriorly flattened and, proportionally, wide element. The proximal process of the *radiale* corresponds to a great part of the proximolateral articular surface, and the proximolateral process develops ventrally until, approximately, the mid portion of the element. The anterior crest of the *radiale* is mildly developed and extends until the mid-portion of the diaphysis. The anteroproximal fossa is less developed and is placed at the proximal portion of the anterior crest. Between the anterior crest and the proximal process, there is a sulcus (medioproximal sulcus) which extends until part of the proximal articular surface. The distal articulation expands laterally in both ways almost in a symmetrical manner, with its medial portion slightly more expanded; its articulation facet is smooth and broad. Examining the *radiale* in posterior view, the ulnar facet of *radiale* is slightly depressed in an oval manner with the proximodistal axis as the largest axis. The ulnar facet of *radiale* is placed at the distal posterior margin of the proximolateral process. The proximal posterior depression is smooth and medially displaced in relation to the proximolateral process.

Ulnare (Figs. 8, 9B). Only the left *ulnare* is preserved and in almost complete. It was associated with the *radiale* before preparation. The *ulnare* has 34 mm of length, 14 mm and 25 mm of width at its proximal and distal articulations, respectively. The diaphysis has an oval cross-section while the proximal articulation has subtriangular shape, with the anteroposterior axis as its major one. The distal articulation has a droplet shaped cross-section with its sharp portion projected medially. The proximal articular surface is flat, and the proximomedial process is well developed, projecting posteromedially and aligned with the medial surface of the element. As for the distal articular surface, there is a smooth and broad concavity, with the distomedial process well-developed, and presenting, on its distoposterior portion, the distal facet for *radiale* articulation.

Distal carpal (Figs. 8, 9C). Both left and right elements are preserved, being the left in better conditions, missing only part of the lateral posterior margin. In dorsal view, the element is rectangular with rounded corners and slightly projected posteriorly. In distal view, the articular ulnar articular facet is well developed and convex. This convexity is best seen in lateral view and its anterior portion is smooth. In distal view, only the Metacarpal III facet is preserved. In the posterior dorsal region, there is a smooth depression, where lies a large foramen.

Metacarpals (Figs. 8, 10A). Nine metacarpals are preserved, five from the left *manus* with three complete elements (MC I-III) and the other two as fragments. And four complete right metacarpals. In general, all metacarpals are robust, but they become thinner and longer toward the digit V. Two general morphologies can be observed: one of thicker metacarpals with its articular facets well-developed seen in metacarpals I-III, and another observed in the metacarpal IV, of longer and thinner elements. Although just one portion of the proximal articular region of the metacarpal V is

preserved, its morphology resembles more the one of metacarpal IV than the morphology of metacarpals I-III. In cross section the diaphysis is oval and slightly compressed dorsoventrally. The proximal articular portion expands anterolaterally, this feature is most evident in metacarpal I. The proximal region is anteriorly rotated about 45° in relation to the distal portion, which, in turn, does not develop much laterally beyond the diaphysis width.

In general, the metacarpals I-III have the proximal region more dorsopalmarly compressed and wider than the diaphysis, having an articular surface approximately flat and more developed in dorsal view than in palmar one. The proximal articular region expands in an anterolateral process. On the metacarpal I, in anterior view, there is a smooth crest at the most proximal portion of the diaphysis dividing a relatively big area of rugose texture for muscular insertion. This area for muscular insertion is restricted to the distolateral portion in the metacarpals II and III, being that, in the latter, this rugose texture occurs in an oval depression. In palmar view, the proximal articulation is slightly concave and present the rugosity for muscular insertion. On the metacarpal I there is a smooth ventromedial crest right above the mid portion of the diaphysis. Those metacarpals (I-III), in dorsal view, possess a shallow distal depression just before the distal articular surface. This articular region develops its dorsal and palmar portions equally, but is less developed in the metacarpal I, and, in general, present a sulcus that divides this articular surface in right and left sides. At the distal articulation, both in lateral and medial views, the articular surface present circular fossae. The metacarpal IV presents a more circular cross-section, with the dorsopalmar section less compressed than those observed in the other metacarpals (I-III). The proximal articular area also develops more dorsally than palmarly and presents the rugosities for muscular insertion described above, but only at the dorsal surface, while the palmar surface is smooth. The distal portion of the metacarpal IV, as well as most part of the proximal portion, diaphysis, and distal portion of the metacarpal V, are not preserved.

Manual phalanges

Medio-proximal phalanges (Figs. 8, 10B-C). The phalanges I-1, II-1, III-1, IV-1, II-2, III-2 of both *manus* and the right phalanges III-3 and IV-1 are preserved. The phalanges from digit I to III have a similar morphology, varying basically in dimensions; with longer proximal elements and shorter distal phalanges. In general, the articular surfaces are expanded while the mid portion have a rectangular cross-section with rounded corners, being wider than taller. The proximal articulation is slightly concave and present a dorsopalmar crest that divides the articular surface in two halves. This crest is not as well developed in the proximal phalanges of the digits I and II as it is in the other preserved digits. In proximal view, the proximal articulation has a subtriangular cross-section. The distal articular surface develops more dorsally than palmarly and have a similar sulcus when compared to that described for the metacarpals, dividing the articular surface in right and left portions. The proximal phalanges have, both in medial and lateral views, circular fossae for muscular insertion at the distal end. The proximal phalange of digit IV does not present the dorsopalmar crest on its proximal articular surface and have a mid-cross-section of subtriangular shape. The distal articulation of these phalanges does not have the sulcus dividing the articular surface in two portions.

Ungual phalanges (Figs. 8, 10D). Five unguinal phalanges are preserved: three left elements (digits I-III) and two right elements (I and II). The general morphology is shared by all elements, being laterally compressed and slightly curved laterally. In lateral view, the unguinal have an approximate triangular profile, with its palmar edge less curved than the dorsal edge. Both in lateral and medial surfaces they present at least one neurovascular foramen located at

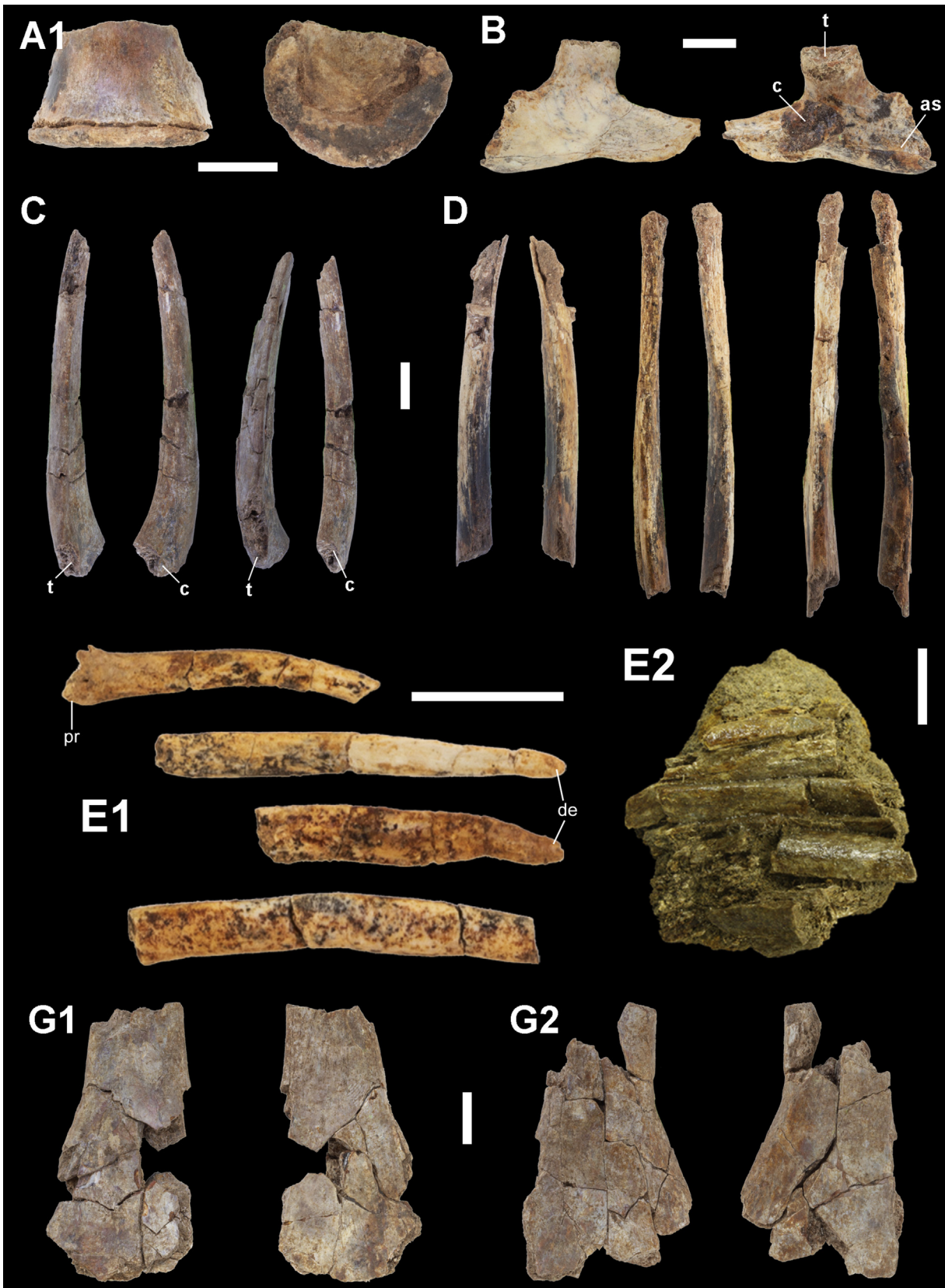


Fig. 5. Elements of the axial skeleton (A–D), gastralia (E), and pelvic girdle (G) of *Armadillosuchus* sp. **A:** A vertebral centrum fragment in dorsoventral (left) and anteroposterior (right) views. **B:** A right cervical rib in lateral (left) and medial (right) views. **C:** Two anterior thoracic ribs in lateral (left) and medial (right) views. **D:** Three posterior thoracic ribs in lateral (left) and medial (right) views. **E:** Isolated (1) and associated (2) elements of the gastralia. **G:** Right (1) and left (2) pubis in dorsal (left) and ventral (right) views. **Abbreviations:** *as* = articular surface for the adjacent cervical rib; *c* = capitulum; *de* = distal end; *pr* = proximal portion *t* = tuberculum. **Scale bars** = 1 cm.

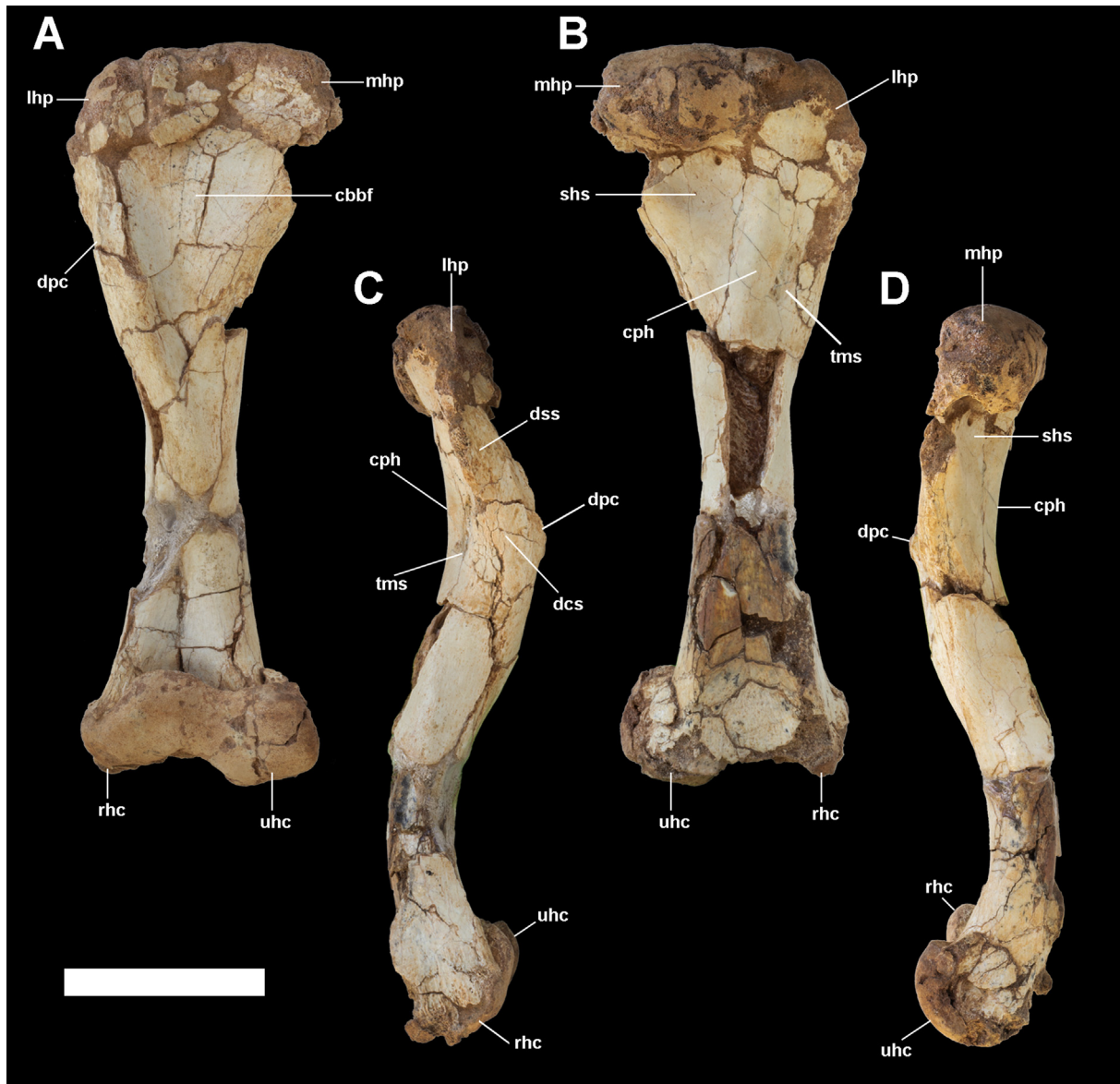


Fig. 6. Right humerus in anterior (A), posterior (B), lateral (C), and medial (D) views. **Abbreviations:** *cbbf* = M. coracobrachialis brevis insertion fossa; *cph* = crest on the posterior surface of the humerus; *dcs* = M. deltoideus clavicularis insertion surface; *dpc* = deltopectoral crest; *dss* = M. deltoideus scapularis insertion scar; *lhp* = lateral humeral process; *mhp* = medial humeral process; *rhc* = radial hemicondyle; *shs* = M. scapulohumeralis insertion surface; *tms* = M. teres major insertion scar; *uhc* = ulnar hemicondyle. **Scale bar** = 5 cm.

the proximal portion, with the medial foramen less developed and more palmarly placed than the lateral foramen. The articular surface is well-developed with dorsal and palmar projections and develops towards the lateral portion of the ungual, so that when articulated with the distalmost phalanx, the ungual is deflected laterally at an angle of approximately 30°. Well-developed keels are present both at the dorsal and palmar margins, being the dorsal keel sharper than the palmar one. These keels and the lateral compression of the ungual gives a blade-like ending to the distal portion.

Pubis (Fig. 5G). Fragments of right and left pubis are preserved, representing part of the diaphysis and distal portion of both elements. A flattening of these elements is observed, which is more pronounced in the distal portion. In cross-section, it is observed that the lateral portion of the pubis is thicker than the medial portion, and, in dorsal view, the lateral margin presents a slight curvature.

Osteoderms (Fig. 11)

The osteoderms were divided into groups according to previous studies (Hill, 2010; Tavares et al., 2015) which have been used for classification of both fossil and living Crocodyliformes. The use of this classification for the present specimen was based on anatomical inferences, which will be discussed later. Not all osteoderms could be associated to one of the proposed groups in the literature because they were anatomically distinct.

Most of the osteoderms were found fragmented or without significant anatomical information that allows their identification and/or orientation. However, 95 complete or partially complete osteoderms, or with relevant anatomical information, were analyzed and divided into groups based on size, shape, and anatomical characteristics. No osteoderm was found articulated with each other or in association with bony elements.

The osteoderms have different dorsal surface shapes, with triangular, rectangular or subrectangular outlines with rounded corners.

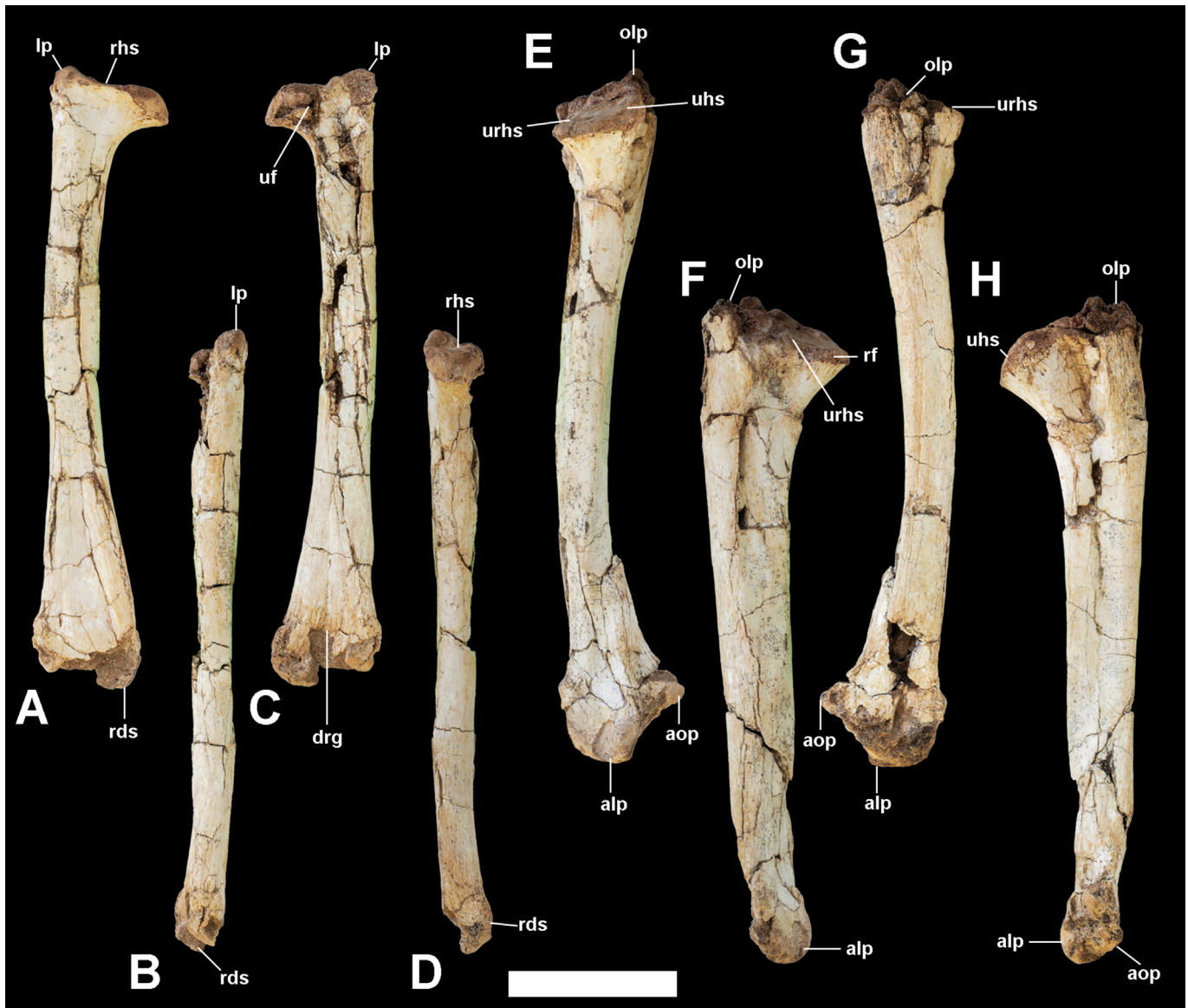


Fig. 7. Right radius and ulna, respectively, in anterior (A and E), lateral (B and F), posterior (C and G) and medial (D and H). **Abbreviations:** *alp* = anterolateral process; *aop* = anterior oblique process; *drg* = distal radial groove; *lp* = lateral process of radiohumeral articular surface; *olp* = olecranon process; *rf* = radial facet; *rhs* = radiohumeral articular surface; *uhs* = ulnar humeral articular surface; *urhs* = ulnar radio humeral articular surface. **Scale bar** = 5 cm.

Some osteoderms have a smooth dorsal surface, but generally the surface is ornamented with pits, grooves, ridges, and tubercles. In some plates this ornamentation follows a radial pattern from the dorsal crest, when this crest is present, to the edges of the plate. The ventral surface has a crisscrossed growth pattern texture. There are neurovascular foramina and, depending on the dermal bone, there may be a posterior articular facet.

Some osteoderms show growth lines arranged horizontally at their margins, when seen marginally. Depending on the preservation status of these plates, the growth lines can be counted, and the largest number found was 12.

Nuchal shield dermal plates (Fig. 11A–C). This group is composed of robust plates with different forms of dorsal surfaces, with suture or smooth margins. Some plates are flattened, but most are dorsoventrally curved. All plates in the group, except one, have the characteristic ornamentation of the dorsal surface, with grooves, pits, and tubercles, but none have the dorsal crest. The ventral surface of these plates does not exhibit the crisscrossed

texture, or at least this feature cannot be observed. Instead, the ventral surface either has a different ornamentation pattern or has a smooth surface, with small depressions, and in some cases with the same typical ornamentation of the dorsal surface. The margins of these plates are sutured and/or smooth, being the smooth margin portions dorsoventrally thinner than the rest of the dermal plate.

Dorsal shield dermal plates (Figs. 11D–F). The osteoderms of this group are predominantly rectangular, broader than long, curved dorsoventrally, and have a lateral projection. This lateral projection may be located more anteriorly or posteriorly. The plates have the characteristic ornamentation of the dorsal surface and a dorsal crest that extends from the posterior margin up to 70% of the anteroposterior length of the osteoderm, fading smoothly in the anterior portion. The crisscrossed pattern of the ventral surface is most evident on these dermal plates. The crosses in this pattern have two obtuse angles that open anteroposteriorly and the most obtuse angle faces anteriorly, while the other posteriorly. All plates

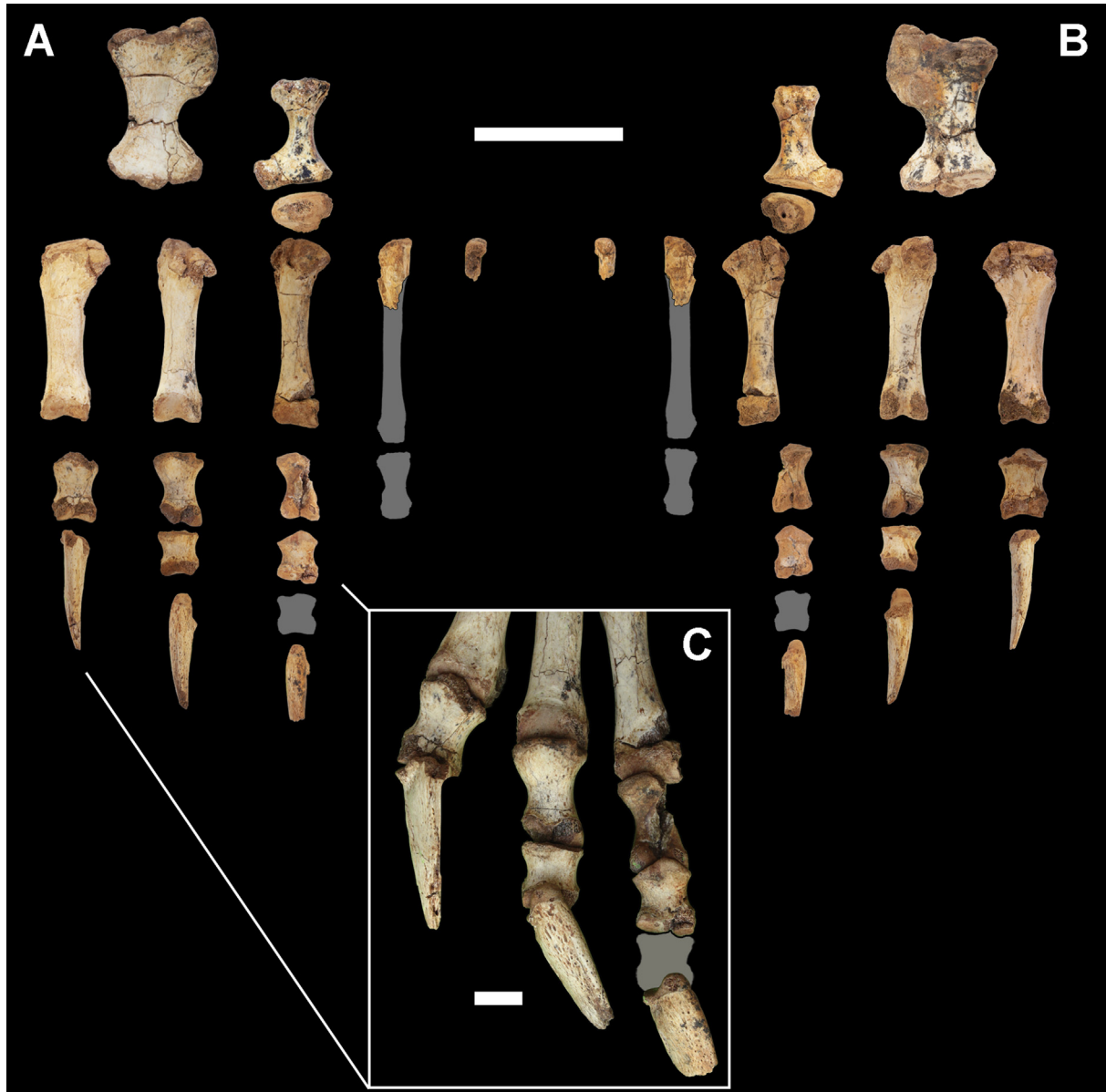


Fig. 8. Preserved elements of the left carpus and manus in dorsal (A) and palmar (B) views. In detail (C), phalangeal articulation. Known, but missing, elements are represented in grey. **Scale bars:** A-B = 5 cm; C = 1 cm.

Table 1
Morphometric measurements of the elements of the right and left manus of *Armadillosuchus* sp. (IFSP-VTP/PALEO-0001).

Element	Total length (mm)					Proximal width (mm)					Distal width (mm)				
	1	2	3	4	5	1	2	3	4	5	1	2	3	4	5
<i>Right manus</i>															
Metacarpal	56.5	56	60.5	64.5	–	27.5	*20	24	–	–	15	15.5	16.5	*9.5	–
Phalanx 1	22	23.5	22	20.5	–	14	16	16	10	–	13	13.5	12.5	*9	–
Phalanx 2	NA	17.5	17	14	–	NA	13.5	12.5	11.5	–	NA	13	13	*11	–
Phalanx 3	NA	NA	13.5	–	–	NA	NA	11.5	–	–	NA	NA	*11.5	–	–
											Proximal height (mm)				
Ungual											21	19	–	–	–
<i>Left manus</i>															
Metacarpal	56.5	58.5	62	–	–	25.5	23	20.5	18	11.5	15.5	15.5	15	–	–
Phalanx 1	22.5	25.5	21.5	–	–	15	15.5	*10.5	–	–	*14	*12.5	12.5	–	–
Phalanx 2	NA	15	17.5	–	–	NA	13.5	12.5	–	–	NA	12.5	12.5	–	–
Phalanx 3	NA	NA	–	–	–	NA	NA	–	–	–	NA	NA	–	–	–
											Proximal height				
Ungual	*36.5	*30	*22.5	–	–	9	8	7.5	–	–	21.5	19	16.5	–	–

Abbreviations and symbols: * = incomplete measure; - = not available; NA = not applicable.

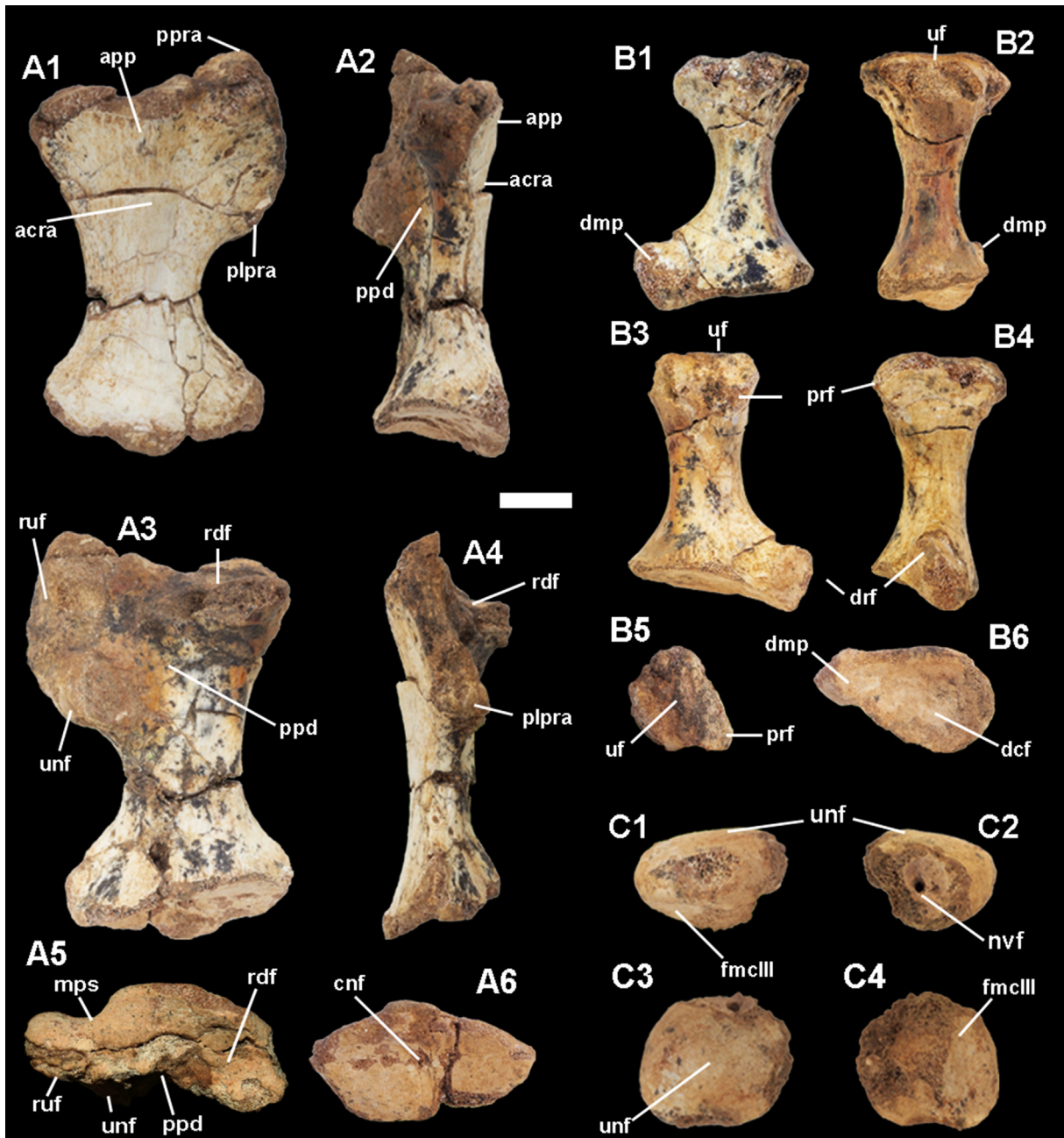


Fig. 9. Elements of the left carpus. **A:** radiale in anterior (A1), lateral (A2), posterior (A3), medial (A4), proximal (A5), and distal (A6) views, respectively. **B:** ulnare in anterior (B1), lateral (B2), posterior (B3), medial (B4), proximal (B5), and distal (B6) views, respectively. **C:** distal carpal in anterior (C1), posterior (C2), proximal (C3), and distal (C4) views, respectively. **Abbreviations:** *acra* = anterior crest of the radiale; *app* = anteroproximal process of the radiale; *cnf* = centrale facet; *dcf* = distal carpal facet; *dmp* = distomedial process of the ulnare; *fmcIII* = metacarpal III facet; *plpra* = lateroproximal process of the radiale; *mpos* = medioproximal sulcus; *ppd* = proximal posterior depression; *ppra* = proximal process of the radiale; *prf* = proximal facet for radiale; *rdf* = radial facet; *ruf* = ulnar facet of radiale; *uf* = ulnar facet of ulnare; *unf* = ulnare facet of radiale. **Scale bar** = 1 cm.

in this group have a prominent articular facet along the entire anterior margin of the plate on their dorsal surface. The posterior margin is smooth and thinner than the rest of the plate except for the portion where the dorsal crest develops. This margin has an articular facet on the ventral surface and forms a shallow depression on this surface. The medial margin is sutured, while the lateral margin is smooth and projects laterally forming the anterolateral process. This process can be located more anteriorly or posteriorly and, the more posterior is the process, the more acute is the projection.

Ventral shield dermal plates (Fig. 11J-M). This group presents flat and rectangular plates that could not be oriented in relation to the largest axis of the specimen. However, the relationship between the sides of these plates is not as pronounced as in the other plates described. The dorsal surface have the characteristic ornamentation described above, with no articular facets in the anterior portion nor the characteristic dorsal crest of the paravertebral plates of the dorsal shield. The ventral surface also follows the standard ornamentation, presenting neither facets of articulation in the posterior portion nor other prominent feature. The sides of these dermal



Fig. 10. Elements of the left manus. **A:** metacarpal I in dorsal (A1), lateral (A2), palmar (A3), medial (A4), proximal (A5), and distal (A6) views, respectively. **B:** medio-proximal phalanx I-1 in dorsal (B1), lateral (B2), palmar (B3), medial (B4), proximal (B5), and distal (B6) views, respectively. **C:** medio-proximal phalanx 1-2 in dorsal (C1), lateral (C2), palmar (C3), medial (C4), proximal (C5), and distal (C6) views, respectively. **D:** unguis phalanx II in lateral (D1), medial (D2), dorsal (D3), and palmar (D4) views, respectively. **Abbreviations:** *alp* = anterolateral process; *crf* = crest on the proximal articular facet; *dphf* = distal phalanx facet of unguis; *nvf* = neurovascular foramina; *pcr* = proximal crest on the dorsal surface; *sdf* = distal articular facet sulcus of metacarpal. **Scale bar:** 1 cm.

plates have edges which form a locking system with the adjacent osteoderms, similar to a puzzle (Fig. 11J-L), and some of these dermal plates have, at least, one of the sides smooth.

Caudal dermal plates (Fig. 11G-I). The osteoderms of this group are flat, rectangular/subtriangular, wider than long, with a sharp lateral expansion of acute angle, which gives a triangular shape to the lateral portion of the plate, similar to a spearhead. The dorsal surface of most of these dermal plates is worn. However, some of them have the typical dorsal ornamentation, but without the dorsal crest and with an anteriorly articular facet proportionally smaller than that seen in dermal plates of the dorsal shield. The

ventral surface of most dermal plates is also worn, and it is possible to see only the neurovascular foramina. Some osteoderms in this group show the typical ornamentation of the ventral surface seen on other dermal plates. However, it is not possible to notice the presence of an articular facet. The medial border of these dermal plates shows sutures, while the lateral borders are sharp and smooth.

Accessory and intercalary dermal plates (Fig. 11N-S). The plates are smaller than all other described ones, being few longer than 2 cm in its greater axis. They are flat but robust, of triangular and/or rounded shape that could not be oriented anteriorly. The dorsal

surface of these dermal plates varies, some have the typical ornamentation, with no crest and articulation facets. Others are smooth due to the wearing process, and some have grooves only in the central portion. The typical ornamentation of the ventral surface is observed in almost all dermal plates, except in those that present more developed wear. The lateral edges of these osteoderms are robust and some have very sharp growth lines.

Possible gastroliths (Fig. 12)

Two pebbles of approximately 2 cm each were found amidst of the sediment. One near the humerus and less than 5 cm from the left manus, and another next to a sequence of three semi-articulated thoracic ribs. These pebbles are interpreted here as possible gastroliths. The largest pebble is made of quartz and the smallest did not have its mineralogical composition determined, but presents at least two types of minerals. In general, they are rounded and slightly flattened. The edges and vertices present well developed polishment, whereas the more depressed regions are more rognose.

5. Phylogenetic analysis

The coded characters for IFSP-VTP/PALEO-0001 represent about 15% of the total characters of the data matrix and contemplate three unambiguous synapomorphies of Sphagesauridae (characters 389-1, 393-1 and 411-1). After the first round of phylogenetic analysis, a total of 99,999 (software limit) trees with 1713 steps were retained. The strict consensus (Fig. 13) of these trees resulted in polytomies at the base of some notosuchian clades, especially within the clade of advanced notosuchians, where *Morrinhosuchus* is the sister clade to a polytomy involving *Llanosuchus tamaensis*, *Coringasuchus anisodontis*, *Labidiosuchus amicum*, *Mariliasuchus amarali*, *Notosuchus terrestris*, IFSP-VTP/PALEO-0001, *Sphagesaurus huenei*, *Armadillosuchus arrudai*, *Caryonosuchus pricei*, *Adamantinasuchus navae*, *Yacararani boliviensis*, and a clade formed by the four *Caipirasuchus* species. Other polytomies were observed in groups comprising basal notosuchians and sebecosuchians. A second analysis was carried out following the same steps, but excluding *Coringasuchus*, *Pehuenchesuchus*, *Pabwehshi*, *Neuquensuchus*, and *Microsuchus* because they were fragmentary taxa with unstable behavior during the search for more parsimonious trees in the present and in previous studies (Pol et al., 2014; Leardi et al., 2015b; Fiorelli et al., 2016; Martinelli et al., 2018).

The new analysis resulted in a total of 360 MPTs with 1698 steps. This result places IFSP-VTP/PALEO-0001 as a member of Sphagesauridae among the group of large-bodied forms, which consists in a clade formed by *Sphagesaurus* as the sister group to a polytomy involving IFSP-VTP/PALEO-001, *Armadillosuchus*, and *Caryonosuchus* (Fig. 14). The exclusion of incomplete taxa resolves not only the general topology of Sphagesauridae, but also most of the polytomies within advanced notosuchians, basal notosuchians, and at the base of sebecosuchia.

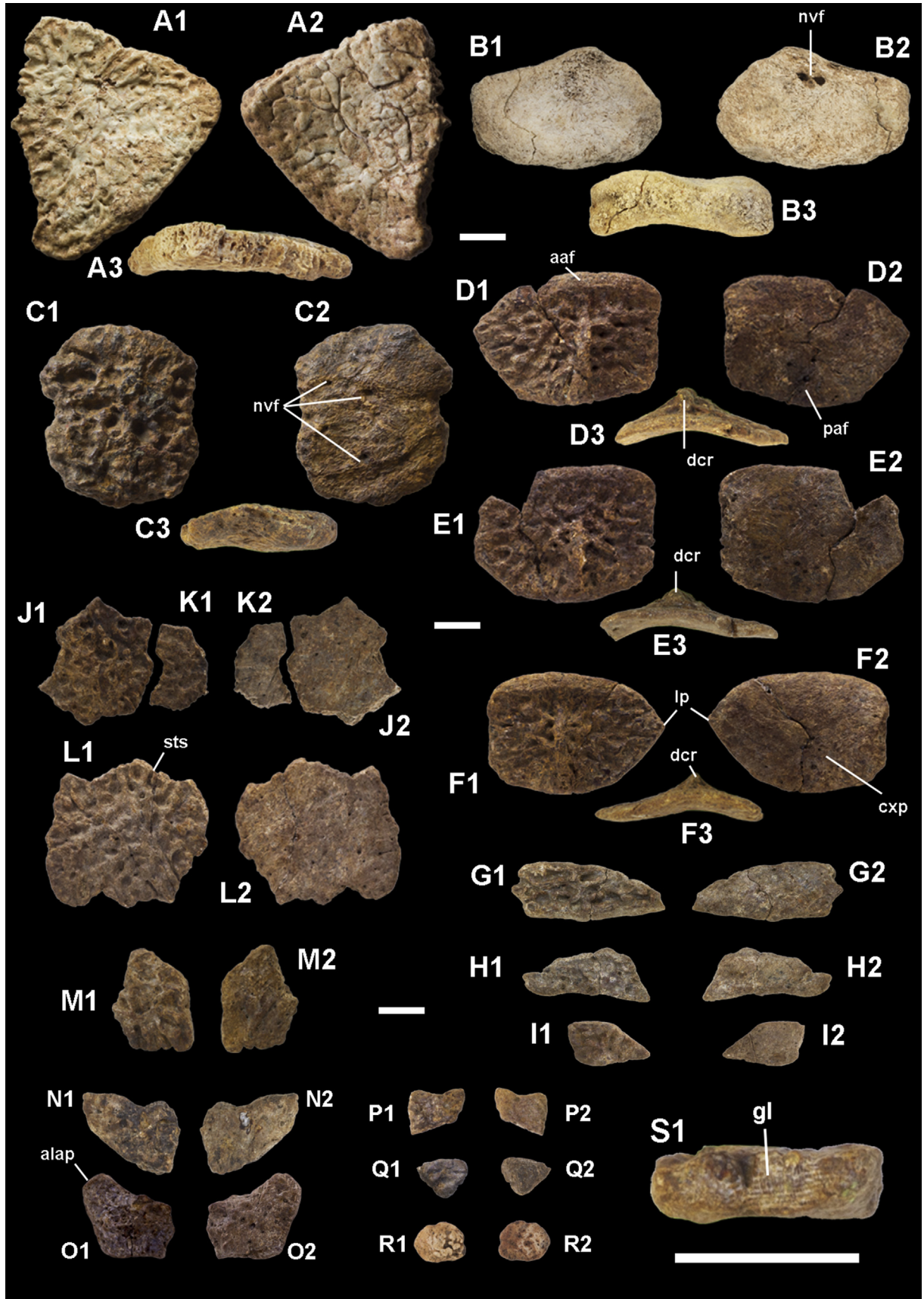
6. Discussion

According to the phylogenetic definition of [Marinho & Carvalho \(2007\)](#), Sphagesauridae is defined as the most inclusive clade of Notosuchia containing *Sphagesaurus hune*i, *Adamantinasuchus navae*, and more related taxa, excluding *Mariliasuchus amarali*, *Uruguaysuchus aznarezi*, *U. terrai*, *Comahuesuchus brachybuccalis*, *Simosuchus clarki*, *Baurusuchus pachecoi*, *Sebecus icaeorhinus*, and *Candidodon itapecuruense*. IFSP-VTP/PALEO-0001 is a member of Sphagesauridae because it appears more closely related to *Sphagesaurus* and *Adamantinasuchus* than to *Mariliasuchus* and *Notosuchus*. This position is observed in all 360 MPTs, when *Coringasuchus*, *Pehuenchesuchus*, *Pabwehshi*, *Neuquensuchus*, and

Microsuchus are excluded from the phylogenetic analysis. The exclusion of these taxa is supported in previous studies ([Pol et al., 2014](#); [Leardi et al., 2015a](#); [Leardi et al., 2015b](#); [Fiorelli et al., 2016](#); [Martinelli et al., 2018](#)) because their anatomical information is incomplete, which means that multiple missing data cells are present in the data matrix. [Wiens \(2003\)](#) states that including taxa with many missing data cells to a phylogenetic data matrix may lead to an increased number of MPTs and unsolved consensus trees. This behavior was observed during the analysis including all taxa. The presence of *Coringasuchus*, *Pehuenchesuchus*, *Pabwehshi*, *Neuquensuchus*, and *Microsuchus* resulted in different topologies within more stable clades, an expressive number of MPTs retained ($n = 99,999$), and an unsolved consensus (Fig. 13). Pruning them from the analysis drastically decrease the number of MPTs ($n = 360$) and improves the accuracy of the consensus (Fig. 14), which, in general, shows the same phylogenetic relationships for Notosuchia presented by [Martinelli et al. \(2018\)](#) with the addition of IFSP-VTP/PALEO-0001 within Sphagesauridae. These results are consistent with the present understanding of the phylogenetic relationships within advanced notosuchians ([Pol et al., 2014](#); [Leardi et al., 2015b](#); [Fiorelli et al., 2016](#)) and adds new information on sphagesaurids, specially about the large-bodied forms ([Nobre & Carvalho, 2006](#); [Andrade & Bertini, 2008](#); [Marinho & Carvalho, 2009](#); [Novas et al., 2009](#); [Iori & Carvalho, 2011](#); [Kellner et al., 2011](#); [Pol et al., 2014](#); [Leardi et al., 2015b](#); [Fiorelli et al., 2016](#); [Iori et al., 2016](#); [Martinelli et al., 2018](#)).

The position of IFSP-VTP/PALEO-001 within Sphagesauridae, and specially within the clade formed by large-bodied sphagesaurids – *Sphagesaurus*, *Caryonosuchus* and *Armadillosuchus* – is supported by three unambiguous synapomorphies of Sphagesauridae (char. 389-1, char. 393-1, and char. 411-1) and one unambiguous synapomorphy of large-bodied sphagesaurids (381-0), out of seven (for Sphagesauridae) and eight (for large-bodied sphagesaurids) unambiguous synapomorphies that had been proposed as diagnoses for these clades ([Pol et al., 2014](#)). Although IFSP-VTP/PALEO-001 has approximately only 15% of all characters scored into the phylogenetic data matrix, lacking crucial information on cranial and mandibular anatomy, it possesses several fragmentary elements or incomplete parts of its skeleton, allowing comparisons of several anatomical aspects of its skeleton with other sphagesaurids. Also, IFSP-VTP/PALEO-0001 bony elements are larger than those of *Adamantinasuchus*, *Yacararani*, and *Caipirasuchus*, suggesting that this crocodyliform is closer related to large-bodied sphagesaurids than to other groups.

In general, IFSP-VTP/PALEO-0001 has the distinctive anatomical features that characterize Sphagesauridae, presenting a dentition with clear differentiation of incisiform, caniniform, and molariform teeth. It is not possible to determine if the incisiform teeth were procumbent in IFSP-VTP/PALEO-0001, but the premaxilla and maxilla fragment preserves a maxillary replacement molariform tooth that shows the mesial rotation pattern seen in the other Sphagesauridae. The wear pattern observed in the IFSP-VTP/PALEO-0001 teeth is also very similar to that observed in other sphagesaurids, presenting in their wear facets sub-horizontal striae, associated in previous studies with a complex chewing system with propalinal movements ([Pol, 2003](#); [Andrade & Bertini, 2008](#); [Iori & Carvalho, 2018](#)). In the teeth of IFSP-VTP/PALEO-0001 it is also possible to observe the same constriction between the root and the crown of the teeth, as seen in other members of the clade ([Pol, 2003](#); [Andrade & Bertini, 2008](#); [Novas et al., 2009](#); [Iori & Carvalho, 2011](#); [Pol et al., 2014](#)), with the exception of *Caipirasuchus mineirus* incisiform and caniniform teeth that lacks a neck or constriction between the crown and root, although its molariforms present this feature ([Martinelli et al., 2018](#)). IFSP-VTP/PALEO-0001 does not present more than one denticulate carina on its molariforms, as



well as the species of *Caipirasuchus*, *Armadillosuchus*, *Caryonosuchus*, and *Sphagesaurus*, but unlike *Adamantinasuchus* and *Yacararani* (Nobre & Carvalho, 2006; Novas et al., 2009; Iori & Carvalho, 2011), which can present up to three carinae.

One of the main differences observed between IFSP-VTP/PALEO-0001 and *Armadillosuchus arrudai* is that in IFSP-VTP/PALEO-0001 the molariform teeth do not present continuous apicobasal ridges on the root surface, being this a characteristic observed only in *A. arrudai* (see Marinho & Carvalho, 2009, Fig. 4).

A new feature for Sphagesauridae and diagnostic for IFSP-VTP/PALEO-0001 is described for the molariform teeth: a pattern of pairs of denticles in the carina, where interdenticular grooves separate pairs of denticles from each other and minor grooves separate denticles within the pairs. This characteristic does not appear to be related to the preservation process or wearing of the teeth in life, since it can also be observed in isolated teeth that present a certain degree of wear and in the maxillary replacement tooth, which does not present wear facets (Figs. 2D, 3).

Small fragments of the premaxilla and maxilla are preserved, with few diagnostic features evident. The lateral surface of these bones is smooth along the alveolar margin, as well as in the other Sphagesauridae, with the presence of neurovascular foramina. IFSP-VTP/PALEO-0001 has the same ornamentation of the dorsal surface of the skull, with grooves, crests, and small pits, observed mainly in the premaxilla and widely described for Notosuchia and Sphagesauridae. In *Caryonosuchus*, this ornamentation presents a different form of this condition in the anterior portion of the rostrum where, in addition to the typical ornamentation, anteroposteriorly aligned tubercles are present (Kellner et al., 2011). In addition, the premaxilla of IFSP-VTP/PALEO-0001 has a protuberance in its posterior portion, which cannot be observed entirely. This feature is interpreted here as the protuberance associated with the hypertrophied caniniform tooth or the lateral expansion of the premaxilla in relation to the maxilla, which is reported in other advanced notosuchians (Pol et al., 2014).

In the posterior fragment of the maxilla, in contact with jugal and lacrimal, a pattern of ornamentation with grooves and pits is observed, similar to that observed in *Armadillosuchus*, but different from that reported for *Caipirasuchus*, *Yacararani*, and *Sphagesaurus*, where this region is smooth or with a less-developed ornamentation pattern (Andrade & Bertini, 2008; Pol et al., 2014). The jugal of IFSP-VTP/PALEO-0001, as well as other Sphagesauridae jugals, does not present in its anterior portion the development of the jugal bar, which is reported for *Sphagesaurus huenei* (Pol, 2003).

No prominent feature is preserved in the fragments of the skull roof – post-orbital and squamosal – of IFSP-VTP/PALEO-0001, except for the typical ornamentation of the dorsal surface already reported, with grooves and pits. In addition, IFSP-VTP/PALEO-0001 does not have evidence of a suprasquamal in this same region, which is described for *Armadillosuchus* (Marinho & Carvalho, 2009).

In general, the preserved mandibular fragments of IFSP-VTP/PALEO-0001 do not show ornamentation in their most lateral and dorsal portions, nor do they give evidences that this characteristic was present; they show only neurovascular foramina piercing the alveolar margin of the dentary. The left mandibular fragment of IFSP-VTP/PALEO-0001 preserves the transition portion of the anterior dental alveoli, which corresponds to the transition from incisiform teeth to molariformes in the mandible, without a lateral

expansion of the alveolar platform, similar to that seen in the large-bodied sphagesaurids, *Armadillosuchus*, *Caryonosuchus*, and *Sphagesaurus*, and different from the pattern observed for the species of *Caipirasuchus* and *Yacararani* and other basal advanced notosuchians, such as *Mariliasuchus* (Pol, 2003; Zaher et al., 2006; Marinho & Carvalho, 2009; Novas et al., 2009; Kellner et al., 2011; Iori et al., 2013; Martinelli et al., 2018).

The surangular and angular of IFSP-VTP/PALEO-0001 preserve the general aspects widely observed in Mesoeucrocodylia, such as the dorsal and ventral tuberosities of the coronoid on the medial surface of the surangular, a fossa and a lateral crest in the angular that extends ventrally along the mandibular fenestra, which is also preserved and described for *Adamantinasuchus*, *Yacararani*, and *Caipirasuchus stenognathus* and *C. mineirus* among the Sphagesauridae (Nobre & Carvalho, 2006; Novas et al., 2009; Pol et al., 2014; Martinelli et al., 2018). Both in these species and in IFSP-VTP/PALEO-0001, this lateral crest develops anteriorly, whereas posteriorly, the lateral crest and the fossa become, respectively, less pronounced and shallow. A clear distinction can be made between the angular of IFSP-VTP/PALEO-0001 and the angular of these species: a descending projection just below the medial ascending process, considered here as the medial descending process (Fig. 4, D2). This characteristic is neither described for *Adamantinasuchus*, *Yacararani*, nor for the two species of *Caipirasuchus*, which are small sphagesaurids, and is described for the first time in a large sphagesaurid. However, this portion of the mandible is not preserved in *Armadillosuchus*, *Caryonosuchus*, and *Sphagesaurus*, which makes it difficult to determine if it is a diagnostic feature of IFSP-VTP/PALEO-0001 as a new species, or a new feature associated with large-bodied sphagesaurids (Nobre & Carvalho, 2006; Novas et al., 2009; Pol et al., 2014; Martinelli et al., 2018). The surangular of IFSP-VTP/PALEO-0001 lacks neurovascular foramina in the anterior dorsal portion, just like *C. paulistanus*, but different to that is observed in the same portion of the surangular of *C. montealtensis*, *C. stenognathus*, and *C. mineirus* which in turn, have at least one similar foramina (Andrade & Bertini, 2008; Iori & Carvalho, 2011; Iori et al., 2013; Pol et al., 2014; Martinelli et al., 2018). As for the remaining Sphagesauridae species, this portion is not preserved.

Few elements of the axial skeleton of IFSP-VTP/PALEO-0001 could be compared, both by their fragmentary nature, as it is the case of the vertebral centrum (Fig. 9A), and by the scarcity of postcranial skeleton elements described for Sphagesauridae in general (Leardi et al., 2015b; Iori et al., 2016). In general, the cervical rib of IFSP-VTP/PALEO-0001 follows that observed in *Yacararani* and *C. montealtensis* (Leardi et al., 2015b; Iori et al., 2016), differing from other notosuchians like *Araripesuchus tsangatsangana* and *Simosuchus clarki* for not having the posterodorsally projecting spine on the posterior process (Turner, 2006; Georgi & Krause, 2010). Unlike what is observed in *Armadillosuchus arrudai*, the dorsal ribs of IFSP-VTP/PALEO-0001 (the ones preserving their proximal region) have thinner anterior and posterior margins. In some cases, the margins are as thin as keels, contrasting with the ribs of *A. arrudai* which have pachyostosis (Marinho & Carvalho, 2009). However, it is worth noting that neither IFSP-VTP/PALEO-0001 nor *Armadillosuchus* fully preserve their dorsal ribs for further and more detailed comparisons.

The pectoral girdle of IFSP-VTP/PALEO-0001 is represented only by a fragment of the coracoid which preserves the coracoid foramen and the anterior margin of the bone in that portion. This oval

Fig. 11. Morphological variation of the osteoderms of *Armadillosuchus* sp. **A-C:** osteoderms of the nuchal shield in dorsal, ventral, and marginal views, respectively. **D-F:** osteoderms of the dorsal shield in dorsal, ventral, and anterior views, respectively. **G-I:** osteoderms of the caudal shield in dorsal and ventral views, respectively. **J-M:** osteoderms of the ventral shield in dorsal and ventral views, respectively. **N-R:** osteoderms of the accessory shield, N and P representing morphotype 1, and Q and R representing morphotype 2. **S:** detail of growthlines on the marginal surface of osteoderms. **Abbreviations:** *aaf* = anterior articular facet; *alalp* = anterolateral articular process; *cxp* = crisscrossed pattern; *dcr* = dorsal crest; *gl* = osteoderm growthlines; *lp* = lateral process; *sts* = sutured marginal surface. **Scale bars:** 1 cm.

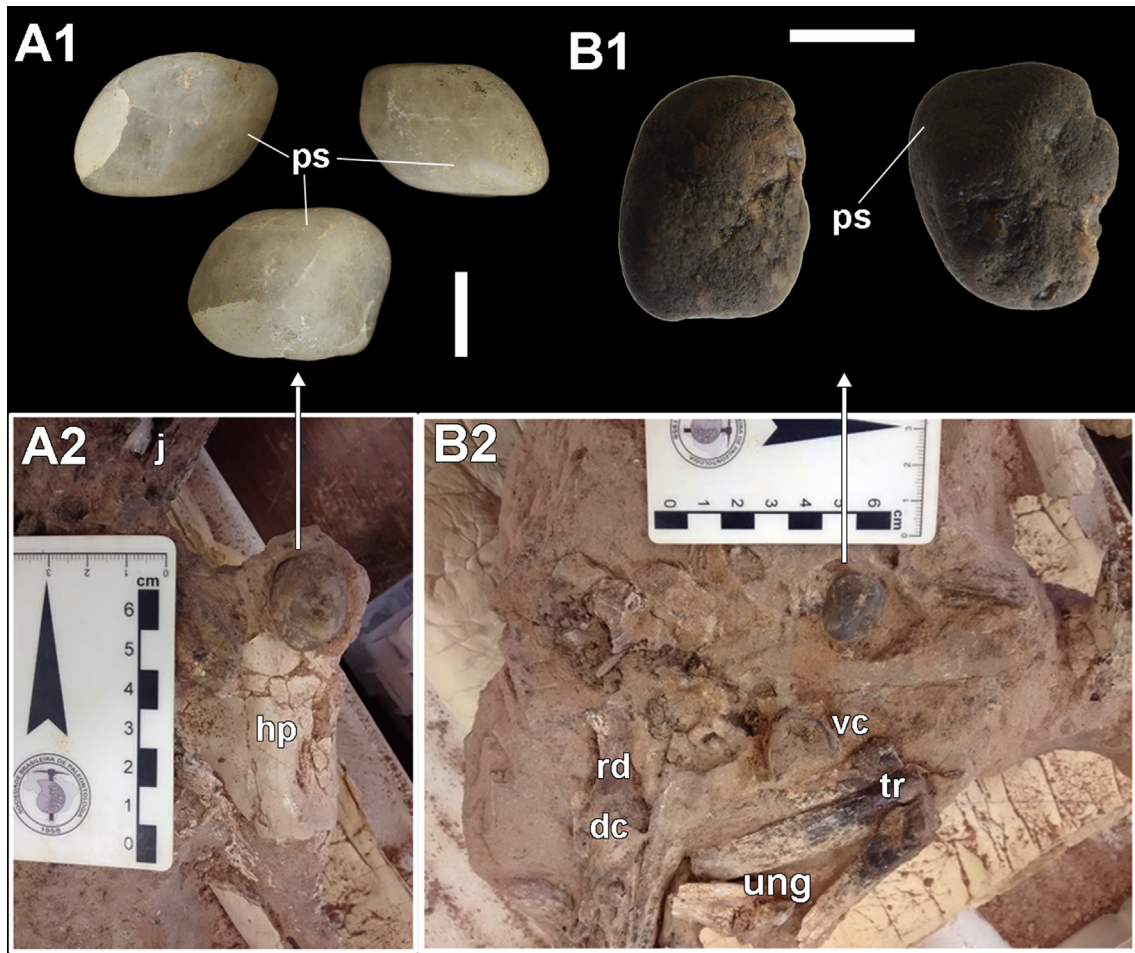


Fig. 12. Two possible gastroliths found in association with *Armadillosuchus* sp. **A1** and **B1**: isolated gastroliths in different views. **A2** and **B2**: gastroliths as they were found during preparation. **Abbreviations:** *dc* = distal carpal; *hp* = humerus proximal portion; *ps* = polished surface; *rd* = radiale; *tr* = thoracic ribs; *ung* = ungual phalanx; *vc* = vertebral centrum. **Scale bars** (A1 and B1) = 1 cm.

and constricted foramen, similar to that described for *C. montealtensis* and *Yacarerani*, is different from the circular foramen described for *Simosuchus*.

In general, the humerus of IFSP-VTP/PALEO-0001 shows the general characteristics already observed in other notosuchians, such as *Araripesuchus tsangatsangana* and sphagesaurids like *Yacarerani*, *Caipirasuchus paulistanus*, *C. montealtensis*, *C. mineirus* and *Armadillosuchus*, having a well developed proximal portion, especially the projection of the medial humeral process, and a deltopectoral crest extending along the entire proximal portion and diaphysis to almost 1/3 of the total humerus length (Turner, 2006; Leardi et al., 2015b; Iori et al., 2016). These features are different from that observed in *Simosuchus*, where the proximal portion is also well developed evenly between the lateral and medial projections of the humerus, and the deltopectoral does not advance distally beyond 1/2 of the humerus length (Sertich & Groenke, 2010). The distal portion of IFSP-VTP/PALEO-0001 humerus also shows the depressions on the anterior and posterior surfaces seen in Mesoeucrocodylia. The anterior depression being markedly deeper than the posterior depression, but as discussed by Leardi et al. (2015b) in *Yacarerani*, this marked depth may be associated with a crushing of this portion, and the same may have happened to IFSP-VTP/PALEO-0001 humerus.

The ulna and radius of IFSP-VTP/PALEO-0001 preserve the general anatomical features observed in Notosuchia, such as ridges

associated with muscular insertion along the surface of the diaphysis and lateromedial projections on its articular surfaces. However, key features in the differentiation of these bones in IFSP-VTP/PALEO-0001 and *Yacarerani*, *Caipirasuchus mineirus* or *Simosuchus* are not well preserved, such as the olecranon process of the ulna and the processes present in the proximal and distal articulations of these bones. However, in the articular portion of the distal epiphysis of the ulna, a sulcus separating anterior and posterior oblique processes is present, being much more developed than those seen in *Yacarerani* and *Simosuchus* (Sertich & Groenke, 2010; Leardi et al., 2015b), but apparently, as observed by Leardi et al. (2015b), the development of this sulcus is associated with a compression of the fossil.

One of the prominent features of IFSP-VTP/PALEO-0001 is the preservation of most carpus and manus bones, which allows the fully observation of the elements (Figs. 8–10). Both the right and left elements are well preserved, with almost all bones present (Table 1, Figs. 8–10). In general, the radial and the ulnar preserve aspects similar to those seen in *Yacarerani* and *Armadillosuchus*. However, IFSP-VTP/PALEO-0001 radials have a well-defined oblique sulcus between the anterior ridge and the proximal process, which is neither seen in the sphagesaurids mentioned above nor in *Simosuchus*. In addition, in proximal view, the proximal articular surface of the radial of IFSP-VTP/PALEO-0001 presents an anteroposterior curvature similar to that seen in *Simosuchus*, but with

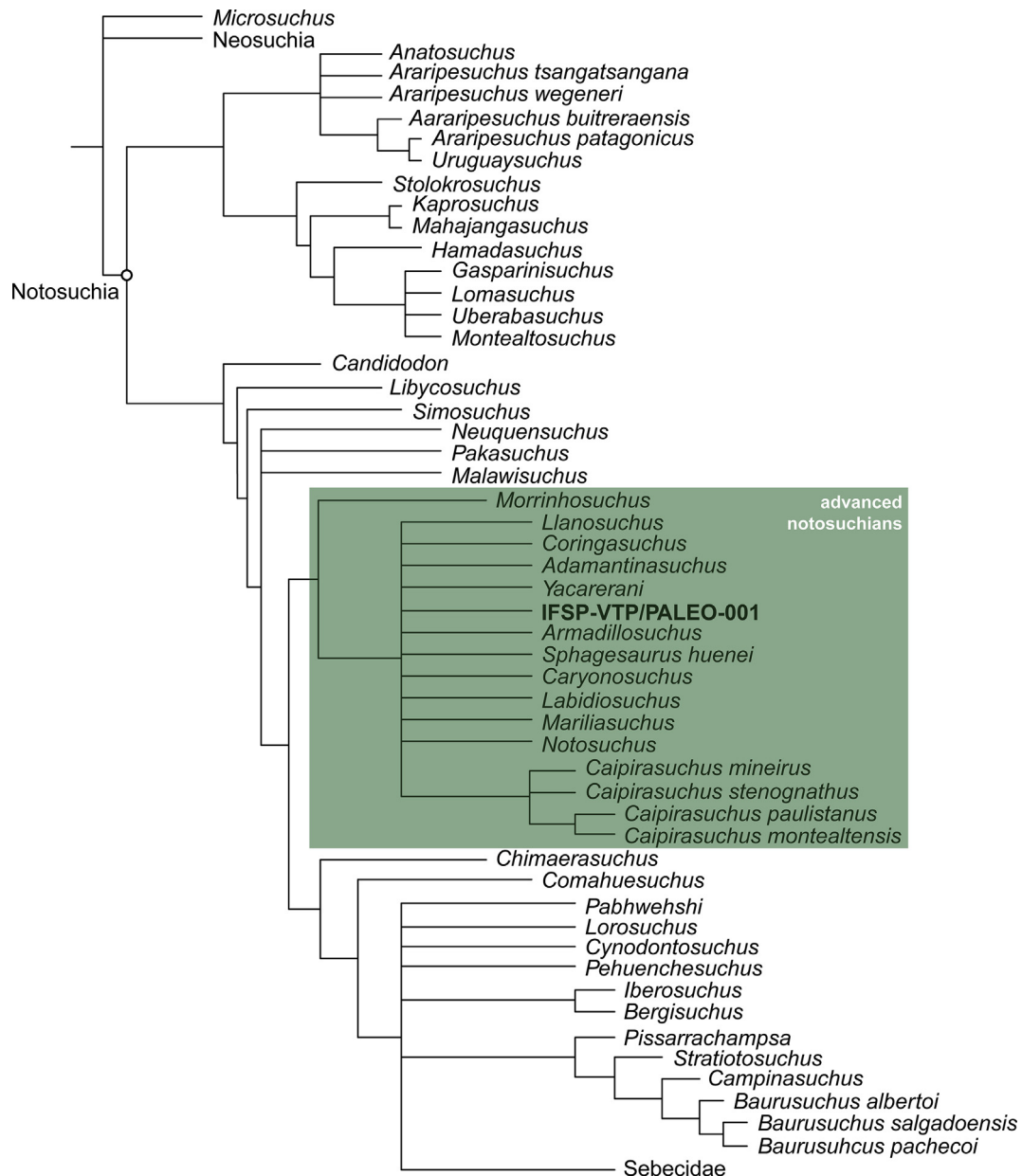


Fig. 13. Phylogenetic relationships of Notosuchia and other mesoeucrocodylians. Strict consensus of all MPTs ($n = 99999$ (overflow), 1713 steps). Some taxa were either pruned or collapsed for the sake of visualization (e.g. Neosuchia, Sebecidae).

its convex portion projected more laterally than the later, and this feature can not be observed in *Armadillosuchus* (Sertich & Groenke, 2010). This same curvature in *Yacarerani* is much more marked than it is in IFSP-VTP/PALEO-0001 and has a crescent-like shape (Leardi et al., 2015b). Although the distal-carpal (dc) of IFSP-VTP/PALEO-0001 does not preserve all the articular surfaces for the metacarpals, it preserves a similar morphology to that seen in the dc IV + V of *Simosuchus*, being rectangular with rounded edges in proximal view and with a slight palmar projection, and preserving the surface for the mc III, but differing from the same distal carpus of *B. albertoi*, which in proximal view is more oval than rectangular (Nascimento & Zaher, 2010). *Yacarerani* also preserves a distal carpus, however, this is interpreted as the dc II + III (Leardi et al., 2015b).

The metacarpals of IFSP-VTP/PALEO-0001 appear to have two basic distinct morphologies: one set of metacarpals have

dorsopalmarly flattened diaphysis with oval cross-sections at their mid-portion, which is seen in mc I-III; and the observed morphology of mc IV, with a thinner and longer diaphysis, which appears to be also present in mc V, given the preserved fragment of this element. In general, this first morphology resembles that observed in *Armadillosuchus*, with the proximal portions of the metacarpals expanding laterally and with a similar width between the diaphysis and the distal articular portions. This pattern is observed in other Notosuchia, such as *Simosuchus*, *Baurusuchus albertoi*, and *Araripesuchus tsangatsangana*, for example (Turner, 2006; Nascimento & Zaher, 2010; Sertich & Groenke, 2010) and the sphagesaurid *Yacarerani boliviensis* (Leardi et al., 2015b). What differs *Armadillosuchus* and IFSP-VTP/PALEO-0001 metacarpals from those of other sphagesaurids is their greater diaphysis width/length ratio, especially if compared to *Yacarerani*, which have longer and thinner metacarpals (Leardi et al., 2015b). The second

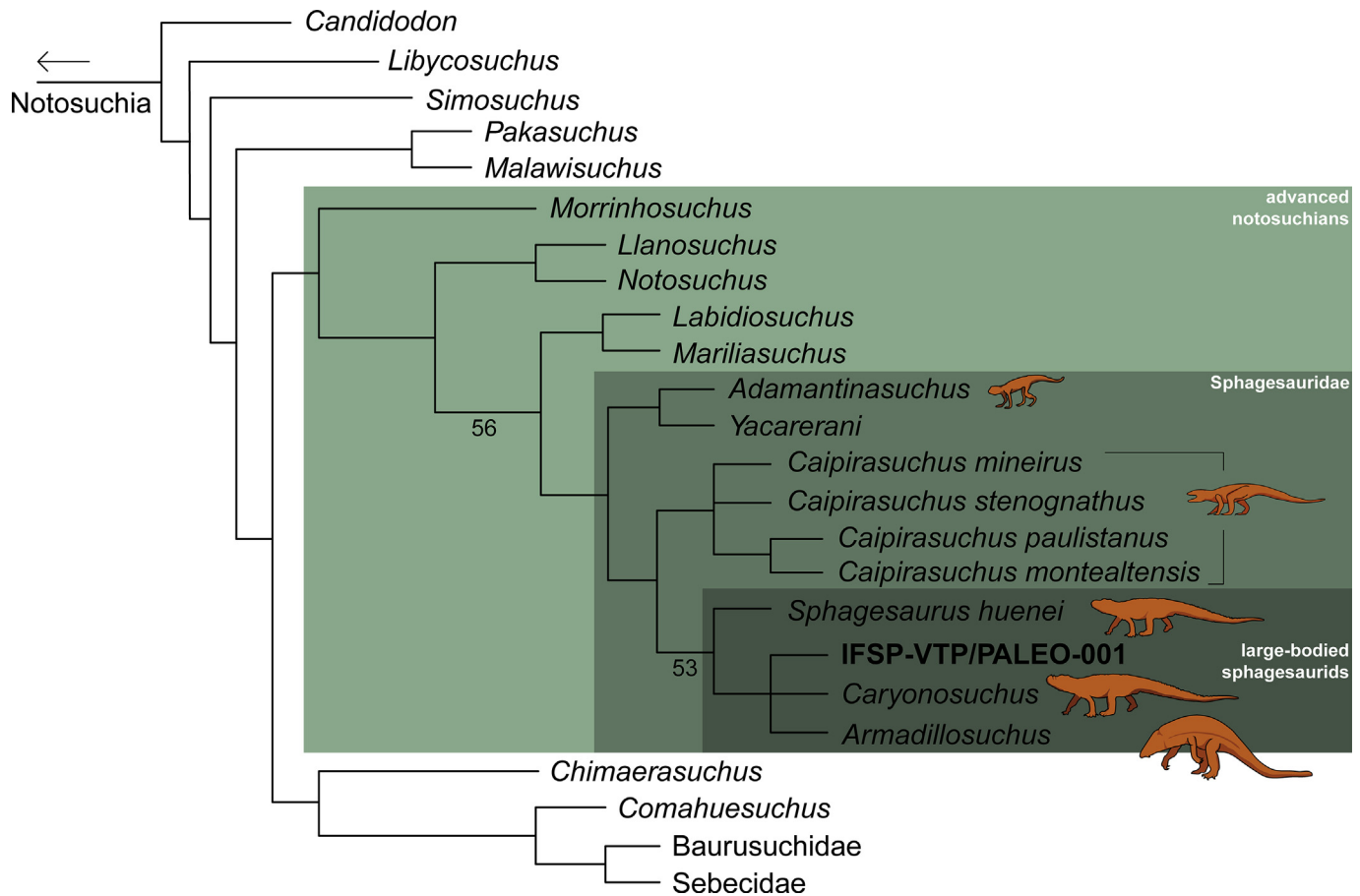


Fig. 14. Phylogenetic relationships of advanced notosuchians and other notosuchians. Strict consensus of all MPTs ($n = 360$, 1698 steps) after pruning *Coringasuchus*, *Pehuenschuchus*, *Pabwehshi*, *Neuquensuchus*, and *Microsuchus*. Some taxa were either pruned or collapsed for the sake of visualization (e.g. Baurusuchidae, Sebecidae). The bootstrap values presented are the absolute frequencies of the monophyletic groups retrieved out of 10000 replicates. Silhouettes represent, respectively, from top to bottom, the general body shape interpreted for *Adamantinasuchus*, *Caipirasuchus* spp., *Sphagesaurus*, *Caryonosuchus*, and *Armadillosuchus*.

morphology described for IFSP-VTP/PALEO-0001 is also different from that observed in *Armadillosuchus*, while in the latter there is no expressive change in the width of the diaphysis toward the metacarpal V. In the former there is a lateral compression of the dorsal surface of the metacarpal, giving a triangular cross-section to the element at the mid-portion.

In general, the phalanges of IFSP-VTP/PALEO-0001 resemble those of *Armadillosuchus* and *Simosuchus*. Like the metacarpals, the medio-proximal phalanges of these crocodyliforms have a greater width/length ratio, being almost as broad as long in the IFSP-VTP/PALEO-0001 phalanx III-4 (Fig. 10B-C), which is different from what is observed in *B. albertoi* and the small sphagesaurid *Yacarerani*, which have longer phalanges. In general, IFSP-VTP/PALEO-0001 ungual phalanges have a lateral curvature with their distal portion protruding laterally. This characteristic is observed in *Simosuchus*, *B. albertoi*, *A. tsangatsangana*, and in the sphagesaurids that preserve their claws: *Yacarerani*, *C. montealtensis*, and *Armadillosuchus*. However, the distal portions of *Armadillosuchus* and IFSP-VTP/PALEO-0001 claws project laterally at an angle of approximately 45° to the proximal articular surface, which in turn, in proximal view, reaches the ungual lateral surface, whereas in the above mentioned notosuchians this feature is not so evident (Leardi et al., 2015b). It is noteworthy that large sphagesaurids such as *Armadillosuchus* and IFSP-VTP/PALEO-0001 share so many carpus and manus characteristics with a non advanced notosuchian, like *Simosuchus*, in some cases even more than with other

sphagesaurids. However, these characteristics may represent homoplasies related to the ecomorphological adaptations of these animals, such as possible adaptations to digging habit (Gomani, 1997; Marinho & Carvalho, 2009; Sertich & Groenke, 2010).

The pelvic girdle of IFSP-VTP/PALEO-0001 is represented by two fragments of the pubis, the right and left basal portion of the blade of the pubis. The fragments appear to have the general characteristics of the elements observed in *Simosuchus*, *B. albertoi*, and *Yacarerani*, having a lateral convexity more pronounced and more proximally located than the medial convexity (Nascimento & Zaher, 2010; Sertich & Groenke, 2010; Leardi et al., 2015b).

Another feature shared among IFSP-VTP/PALEO-0001, *Armadillosuchus*, and *Simosuchus* is the presence of a complex system of osteoderms that, in general, are made up of plates of different morphologies that can be associated with different parts of the body or dermal shields. *Simosuchus* osteoderms have a general rectangular shape in almost all elements, which may have sutured margins or articular surfaces, as well as *Montealtosuchus arrudacamposi* (Hill, 2010; Tavares et al., 2015). The dermal plates of IFSP-VTP/PALEO-0001 have a greater variety of shapes if compared to other sphagesaurids, including the rectangular dermal plates with lateral projections of the parasagittal shield observed in *Caipirasuchus montealtensis* and *C. paulistanus* (Iori et al., 2016), but lacking the d-shaped and non-imbricated plates present in the presacral region of *C. mineirus* (Martinelli et al., 2018). IFSP-VTP/PALEO-0001 and *Armadillosuchus* also share thicker osteoderms

in the nuchal shield, which are attached to each other by sutures. Although the dermal plates of IFSP-VTP/PALEO-0001 are isolated, the diversity of forms and number of preserved elements is one of the highest among the described species of Notosuchia.

The isolated pebbles associated with IFSP-VTP/PALEO-0001 were determined as possible gastroliths because they met some sedimentological and taphonomic requirements, such as: been found *in situ*, having a much coarser granulometry than that of the sedimentary matrix which involved the fossil, and they were associated with articulated skeletons (Wings, 2004). However, a crucial parameter for the determination of fossil gastroliths is not attended, because they are not preserved in association with gastric elements or stomach content. Even though this last parameter is essential for an unambiguous determination of fossil gastroliths, it is worth noting that IFSP-VTP/PALEO-0001 elements were moved during taphonomic processes, but not in an expressive way, since many of the elements were found close to their correct anatomical positions. Although this determination is ambiguous, it is important, during the process of fossil preparation, to pay special attention to such pebbles, since gastroliths can add important information about the diet of fossilised animals or other habits in life.

When analyzing the diagnostic characteristics of the Sphagesauridae genera which can be compared with IFSP-VTP/PALEO-0001, it is possible to observe several points of intersection that characterize this specimen as a sphagesaurid, especially in dentition related characteristics that are observed in all sphagesaurids, such as the paramesial rotation of maxillary teeth of these animals (Andrade & Bertini, 2008; Marinho & Carvalho, 2009; Iori & Carvalho, 2011; Kellner et al., 2011; Pol et al., 2014; Leardi et al., 2015b; Iori et al., 2016). Moreover, when we look into the diagnoses of the genera of large sphagesaurids – *Armadillosuchus*, *Caryonosuchus*, *Sphagesaurus* –, we see that those synapomorphies described for *Armadillosuchus* fit best in what is possible to be observed in IFSP-VTP/PALEO-0001, even though IFSP-VTP/PALEO-0001 presents only two preserved premaxillary teeth like *Sphagesaurus* and *Caryonosuchus*.

Among the synapomorphies of *Armadillosuchus* shared by IFSP-VTP/PALEO-0001 is the presence of immobile dermal shields with sutured and hexagonal dermal plates, dermal plates with different morphologies, and the possibility of two or more premaxillary teeth (Marinho & Carvalho (2009); Marinho, personal communication). The number of premaxillary teeth may not be a strong diagnostic characteristic, as variation in this number is commonly reported in crocodylomorphs, including living forms and in Sphagesauridae, where new specimens of *Armadillosuchus* present three premaxillary teeth (Marinho, personal communication), and Iori et al. (2013), when proposing the reclassification of *Sphagesaurus montealtensis* as *Caipirasuchus montealtensis*, describe a new specimen (MPMA 67-0001/00) with four premaxillary teeth and not only two, as observed in the holotype (Andrade & Bertini, 2008; Iori et al., 2013).

As well as the analysis of the diagnostic characteristics of large sphagesaurids, the morphological comparisons point to a greater affinity of IFSP-VTP/PALEO-0001 to the genus *Armadillosuchus*. Those comparisons are related to the elements of the postcranial skeleton, such as forms and proportions of the elements of the anterior limb, especially the *autopodium*; and the dermal plates, such as different types of attachment (sutured and imbricated), the different morphology of osteoderms, and the possible presence of at least two distinct dermal shields based on the osteoderms morphologies, with an immobile cervical shield, of sutured osteoderms, and a banded (“armadillo-like”) dorsocervical shield, with imbricated parasagittal osteoderms. Nevertheless, IFSP-VTP/PALEO-0001 presents diagnostic features that differentiate it from

Armadillosuchus arrudai and all other sphagesaurids, like the pattern of paired-denticles in the keel of molariform teeth, the medial descending process of the angular, the medial-proximal groove of the radial and the new described morphologies for its osteoderms. Thus, its association to the genus *Armadillosuchus* is well supported, but the distinction between *A. arrudai* is clear. However, the formal description of a new species is precluded because it is a rather fragmentary specimen, with few elements in association that actually represent the anatomy of this animal. Based on these points, we suggest that the specimen herein described, IFSP-VTP/PALEO-0001, should be referred as *Armadillosuchus* sp.

7. Conclusion

From an anatomical point of view, *Armadillosuchus* sp. (IFSP-VTP/PALEO-0001) has the unique dental morphology of Sphagesauridae, as well as a greater similarity of its postcranial elements with those of *Armadillosuchus arrudai*, and also has anterior limbs with a larger ratio between the width of the diaphysis and the total length of the bones, as well as ungueal phalanges evidently laterally curved and having a laterally displaced proximal articular facet. These anatomical characteristics allow the scoring of key characters for the reconstruction of internal relationships in Sphagesauridae and place *Armadillosuchus* sp. within this group and among the large-bodied forms. However, IFSP-VTP/PALEO-0001 is nested in a polytomy comprising *Caryonosuchus pricei* and *Armadillosuchus arrudai*. New records of this sphagesaurid and others are needed to solve these ambiguous relationships and to allow the formal description of the species and as well as to provide data for studies exploring morphofunctional or ecological aspects of these sphagesaurids.

The new materials described in this paper, which include new information on the anatomy of large-bodied sphagesaurids – such as the mandible, elements of the axial skeleton and osteoderms – may contribute to the elaboration of new characteristics for future phylogenetic analyzes of the group. This may corroborate the existence of a monophyletic group of large-bodied sphagesaurids, together with *Sphagesaurus*, *Armadillosuchus*, and *Caryonosuchus*, within the family Sphagesauridae.

The possible presence of gastroliths associated to IFSP-VTP/PALEO-0001 can provide more clues on the alimentary diet of this group of advanced notosuchians. In this sense, it is worth noting that more attention should be given to the work of collecting and preparing new materials, since there is no determining characteristic for the identification of these materials in the fossil record, except for their position in relation to the preserved skeleton. In this case, true gastroliths can be misinterpreted as ordinary pebbles.

Acknowledgments

We thank Hussam Zaher and Alberto B. Carvalho (Museu de Zoologia da Universidade de São Paulo - MZUSP) and Thiago Marinho (Museu dos Dinossauros and Centro de Pesquisas Paleontológicas Llewellyn Ivor Price - UFTM) for access to the collections under their care. We also thank Thiago Marinho and an anonymous reviewer for their comments that improved an earlier version of this manuscript. This study was financed in part by the Coordenação de Aperfeiçoamento de Pessoal de Nível Superior – Brazil (CAPES) – Finance code 001. RMS also thanks the *Conselho Nacional de Desenvolvimento Científico e Tecnológico* (National Council for Scientific and Technological Development) for supporting this research (process 401784/2010-0).

References

- Andrade, M.B., Bertini, R., 2008. A New *Sphagesaurus* (Mesoeucrocodylia: Notosuchia) from the Upper Cretaceous of Monte Alto City (Bauru Group, Brazil), and a Revision of the Sphagesauridae. *Historical Biology* 20 (2), 101–136. <https://doi.org/10.1080/08912960701642949>.
- Basilici, G., Dal'bo, P.F., De Oliveira, E.F., 2016. Distribution of palaeosols and deposits in the temporal evolution of a semiarid fluvial distributary system (Bauru Group, Upper Cretaceous, SE Brazil). *Sedimentary Geology* 341, 245–264, 0037-0738.
- Batezelli, A., 2010. Arcabouço Tectono-estratigráfico e Evolução das Bacias Caiuá e Bauru no Sudeste Brasileiro. *Revista Brasileira de Geociências* 40 (2), 265–285, 0375-7536.
- Batezelli, A., 2017. Continental systems tracts of the Brazilian Cretaceous Bauru Basin and their relationship with the tectonic and climatic evolution of South America. *Basin Research* 29 (1–25), 0950-091X.
- Batezelli, A., Saad, A.R., De Carlos, M.L., 2003. Análise estratigráfica aplicada à Formação Araçatuba (Grupo Bauru-Ks) no centro-oeste do estado de São Paulo. *Geociências* 22, 5–19.
- Candeiro, C.R.A., Rich, T.H., 2010. Overview of the Late Cretaceous biota of the western São Paulo State, Brazil, Bauru Group. *Journal of South American Earth Sciences* 29 (2), 346–353. <https://doi.org/10.1016/j.jsames.2009.08.001>.
- Castro, M.C., Goin, F.J., Ortiz-Jaureguizar, E., Vieytes, E.C., Tsukui, K., Ramezani, J., Batezelli, A., Marsola, J.C.A., Langer, M.C., 2018. A Late Cretaceous mammal from Brazil and the first radioisotopic age for the Bauru Group. *Royal Society Open Science* 5 (5). <https://doi.org/10.1098/rsos.180482>.
- Dias-Brito, D., Musacchio, E.A., De Castro, J.C., Maranhão, M.S.a.S., Suárez, J.M., Rodrigues, R., 2001. Grupo Bauru: uma unidade continental do Cretáceo no Brasil-concepções baseadas em dados micropaleontológicos, isotópicos e estratigráficos. *Revista de Paleobiologia* 20 (1), 245–304, 0253-6730.
- Fernandes, L.A., 1998. Estratigrafia e evolução geológica da parte oriental da Bacia Bauru (Ks, Brasil). Instituto de Geociências, Universidade de São Paulo, 272 p.
- Fernandes, L.A., Coimbra, A.M., 1996. A Bacia Bauru (Cretáceo Superior, Brasil). *Anais da Academia Brasileira de Ciências* 68 (2), 195–206, 0001-3765.
- Fernandes, L.A., Coimbra, A.M., 2000. Revisão estratigráfica da parte oriental da bacia Bauru (Neocretáceo). *Revista Brasileira de Geociências* 30 (4), 717–728.
- Fiorelli, L.E., Leardi, J.M., Hechenleitner, E.M., Pol, D., Basilici, G., Grellet-Tinner, G., 2016. A new Late Cretaceous crocodyliform from the western margin of Gondwana (La Rioja Province, Argentina). *Cretaceous Research* 60, 194–209. <https://doi.org/10.1016/j.cretres.2015.12.003>.
- Garcia, A.J.V., Rosa, A.A.S., Goldberg, K., 2005. Paleoenvironmental and Paleoclimatic Control on Early Diagenetic Processes and Fossil Record in Cretaceous continental Sandstones of Brazil. *Journal of South American Earth Sciences* 19 (3), 243–258. <https://doi.org/10.1016/j.jsames.2005.01.008>.
- Gasparini, Z.B., 1971. Los Notosuchia del Cretácico de América del Sur como un nuevo infraorden de los Mesosuchia (Crocodylia). *Ameghiniana* 8 (2), 83–103, 1851-8044.
- Georgi, J.A., Krause, D.W., 2010. Postcranial axial skeleton of *Simosuchus clarki* (Crocodyliformes: Notosuchia) from the Late Cretaceous of Madagascar. *Journal of Vertebrate Paleontology* 30 (Suppl. 1), 99–121. <https://doi.org/10.1080/02724634.2010.519172>.
- Gobbo-Rodrigues, S.R., Petri, S., Bertini, R.J., 1999. Ocorrências de ostrácodos na Formação Adamantina do Grupo Bauru, Cretáceo Superior da Bacia do Paraná e possibilidades de correlação com depósitos isócronos argentinos. Parte I—Família Ilyocyprididae. *Acta Geologica Leopoldensia* 23 (49), 3–13.
- Goldberg, K., Garcia, A.J.V., 2000. Palaeobiogeography of the Bauru Group, a Dinosaur-Bearing Cretaceous Unit, Northeastern Parana Basin, Brazil. *Cretaceous Research* 21 (2–3), 241–254. <https://doi.org/10.1006/cres.2000.0207>.
- Goloboff, P.A., Santiago, A.C., 2016. TNT version 1.5, including a full implementation of phylogenetic morphometrics. *Cladistics* 32 (3), 221–238. <https://doi.org/10.1111/cla.12160>.
- Gomani, E.M., 1997. A crocodyliform from the Early Cretaceous dinosaur beds, northern Malawi. *Journal of Vertebrate Paleontology* 17 (2), 280–294, 0272-4634.
- Granot, R., Dymant, J., Gallet, Y., 2012. Geomagnetic field variability during the Cretaceous Normal Superchron. *Nature Geoscience* 5 (3), 220, 1752-0908.
- Hay, O.P., 1930. Second bibliography and catalogue of the fossil vertebrata of North America.
- Hill, R.V., 2010. Osteoderms of *Simosuchus clarki* (Crocodyliformes: Notosuchia) from the Late Cretaceous of Madagascar. *Journal of Vertebrate Paleontology* 30 (Suppl. 1), 154–176. <https://doi.org/10.1080/02724634.2010.518110>.
- Iori, F.V., Carvalho, I.S., 2011. *Caipirasuchus paulistanus*, a new sphagesaurid (Crocodylomorpha, Mesoeucrocodylia) from the Adamantina Formation (Upper Cretaceous, Turonian–Santonian), Bauru Basin, Brazil. *Journal of Vertebrate Paleontology* 31 (6), 1255–1264. <https://doi.org/10.1080/039.031.0601>.
- Iori, F.V., Carvalho, I.S., 2018. The Cretaceous crocodyliform *Caipirasuchus*: behavioral feeding mechanisms. *Cretaceous Research* 84, 181–187. <https://doi.org/10.1016/j.cretres.2017.11.023>.
- Iori, F.V., Carvalho, I.S., Marinho, T.S., 2016. Postcranial skeletons of *Caipirasuchus* (Crocodyliformes, Notosuchia, Sphagesauridae) from the Upper Cretaceous (Turonian–Santonian) of the Bauru Basin, Brazil. *Cretaceous Research* 60, 109–120. <https://doi.org/10.1016/j.cretres.2015.11.017>.
- Iori, F.V., Marinho, T.S., Carvalho, I.S., Campos, A.C.A., 2013. Taxonomic reappraisal of the sphagesaurid crocodyliform *Sphagesaurus montealtensis* from the Late Cretaceous Adamantina Formation of São Paulo State, Brazil. *Zootaxa* 3686 (2), 183–200. <https://doi.org/10.11646/zootaxa.3686.2.4>.
- Kellner, A.W.A., Campos, D.A., Riff, D., Andrade, M.B., 2011. A New Crocodylomorph (Sphagesauridae, Notosuchia) with Horn-Like Tubercles from Brazil. *Zoological Journal of the Linnean Society* 163, S57–S65. <https://doi.org/10.1111/j.1096-3642.2011.00712.x>.
- Kley, N.J., Sertich, J.J.W., Turner, A.H., Krause, D.W., O'connor, P.M., Georgi, J.A., 2010. Craniofacial morphology of *Simosuchus clarki* (Crocodyliformes: Notosuchia) from the Late Cretaceous of Madagascar. *Journal of Vertebrate Paleontology* 30 (Suppl. 1), 13–98. <https://doi.org/10.1080/02724634.2010.532674>.
- Kuhn, O., 1968. *Die Vorzeitlichen Krokodile*. Krailling bei München: Oebe.
- Leardi, J.M., Fiorelli, L.E., Gasparini, Z.B., 2015a. Redescription and reevaluation of the taxonomical status of *Microsuchus schilleri* (Crocodyliformes: Mesoeucrocodylia) from the Upper Cretaceous of Neuquén, Argentina. *Cretaceous Research* 52, 153–166. <https://doi.org/10.1016/j.cretres.2014.09.007>.
- Leardi, J.M., Pol, D., Novas, F.E., Suárez, R.M., 2015b. The postcranial anatomy of *Yacarerani boliviensis* and the phylogenetic significance of the notosuchian postcranial skeleton. *Journal of Vertebrate Paleontology* 35 (6), e995187. <https://doi.org/10.1080/02724634.2014.995187>.
- Marinho, T.S., Carvalho, I.S., 2007. Revision of the Sphagesauridae Kuhn, 1968 (Crocodyliformes, Mesoeucrocodylia). *Cenários de Vida, Paleontologia*, pp. 481–487.
- Marinho, T.S., Carvalho, I.S., 2009. An armadillo-like sphagesaurid crocodyliform from the Late Cretaceous of Brazil. *Journal of South American Earth Sciences* 27 (1), 36–41. <https://doi.org/10.1016/j.jsames.2008.11.005>.
- Martinelli, A.G., Marinho, T.S., Iori, F.V., Ribeiro, L.C.B., 2018. The first *Caipirasuchus* (Mesoeucrocodylia, Notosuchia) from the Late Cretaceous of Minas Gerais, Brazil: new insights on sphagesaurid anatomy and taxonomy. *PeerJ* 6, e5594. <https://doi.org/10.7717/peerj.5594>.
- Nascimento, P.M., Zaher, H., 2010. A new species of *Baurusuchus* (Crocodyliformes, Mesoeucrocodylia) from the Upper Cretaceous of Brazil, with the first complete postcranial skeleton described for the family Baurusuchidae. *Papéis Avulsos de Zoológico* 50, 323–361, 0031-1049.
- Nobre, P.H., Carvalho, I.S., 2006. *Adamantinasuchus navae*: a new gondwanan Crocodylomorpha (Mesoeucrocodylia) from the Late Cretaceous of Brazil. *Gondwana Research* 10 (3–4), 370–378. <https://doi.org/10.1016/j.jgr.2006.05.008>.
- Novas, F.E., Pais, D.F., Pol, D., Carvalho, I.S., Scanferla, A., Mones, A., Riglos, M.S., 2009. Bizarre notosuchian crocodyliform with associated eggs from the Upper Cretaceous of Bolivia. *Journal of Vertebrate Paleontology* 29 (4), 1316–1320. <https://doi.org/10.1671/039.029.0409>.
- Pol, D., 2003. New remains of *Sphagesaurus huenei* (Crocodylomorpha: Mesoeucrocodylia) from the Late Cretaceous of Brazil. *Journal of Vertebrate Paleontology* 23 (4), 817–831. <https://doi.org/10.1671/a1015-7>.
- Pol, D., 2005. Postcranial remains of *Notosuchus terrestris* Woodward (Archosauria: Crocodyliformes) from the upper Cretaceous of Patagonia, Argentina. *Ameghiniana* 42 (1), 21–38, 1851-8044 (on-line).
- Pol, D., Nascimento, P.M., Carvalho, A.B., Riccomini, C., Pires-Domingues, R.A., Zaher, H., 2014. A new notosuchian from the Late Cretaceous of Brazil and the phylogeny of advanced notosuchians. *PLoS One* 9 (4), e93105. <https://doi.org/10.1371/journal.pone.0093105>.
- Santucci, R.M., Bertini, R.J., 2001. Distribuição paleogeográfica e biocronológica dos titanossauros (Saurischia, Sauropoda) do Grupo Bauru, Cretáceo Superior do sudeste brasileiro. *Revista Brasileira de Geociências* 31 (3), 307–314, 0375-7536.
- Sertich, J.J.W., Groenke, J.R., 2010. Appendicular skeleton of *Simosuchus clarki* (Crocodyliformes: Notosuchia) from the Late Cretaceous of Madagascar. *Journal of Vertebrate Paleontology* 30 (Suppl. 1), 122–153. <https://doi.org/10.1080/02724634.2010.516902>.
- Tamrat, E., Ernesto, M., Fulfaro, V.J., Saad, A.R., Batezelli, A., Oliveira, A.F., 2002. Magnetoestratigrafia das formações Uberaba e Marília (Grupo Bauru) no triângulo mineiro (MG). VI Simpósio sobre o Cretáceo do Brasil, São Pedro, Brasil, pp. 323–327.
- Tavares, S.a.S., 2007. *Montealtosuchus arrudacamposi*, a new peirosaurid crocodile (Mesoeucrocodylia) from the Late Cretaceous Adamantina Formation of Brazil. *Zootaxa* 1607, 35–46.
- Tavares, S.a.S., Ricardi-Branco, F., Carvalho, I.S., 2015. Osteoderms of *Montealtosuchus arrudacamposi* (Crocodyliformes, Peirosauridae) from the Turonian–Santonian (Upper Cretaceous) of Bauru Basin, Brazil. *Cretaceous Research* 56, 651–661. <https://doi.org/10.1016/j.cretres.2015.07.002>.
- Tavares, S.a.S., Ricardi-Branco, F., Carvalho, I.S., Maldanis, L., 2017. The morpho-functional design of *Montealtosuchus arrudacamposi* (Crocodyliformes, Upper Cretaceous) of the Bauru Basin, Brazil. *Cretaceous Research* 79, 64–76. <https://doi.org/10.1016/j.cretres.2017.07.003>.
- Turner, A.H., 2006. Osteology and phylogeny of a new species of *Araripesuchus* (Crocodyliformes: Mesoeucrocodylia) from the Late Cretaceous of Madagascar. *Historical Biology* 18 (3), 255–369. <https://doi.org/10.1080/08912960500516112>.
- Walker, A.D., 1970. A revision of the Jurassic reptile *Hallopus victor* (Marsh), with remarks on the classification of crocodiles. *Philosophical Transactions of the Royal Society of London B Biological Sciences* 257 (816), 323–372. <https://doi.org/10.1098/rstb.1970.0028>.
- Whetstone, K.N., Whybrow, P., 1983. A cursorial crocodylian from the Triassic of Lesotho (Basutoland), South Africa. University of Kansas Museum of Natural History, p. 106. Occasional Paper.

- Wiens, J.J., 2003. Incomplete taxa, incomplete characters, and phylogenetic accuracy: is there a missing data problem? *Journal of Vertebrate Paleontology* 23 (2), 297–310. [https://doi.org/10.1671/0272-4634\(2003\)023\[0297:iticap\]2.0.co;2](https://doi.org/10.1671/0272-4634(2003)023[0297:iticap]2.0.co;2).
- Wings, O., 2004. Identification, distribution, and function of gastroliths in dinosaurs and extant birds with emphasis on ostriches (*Struthio camelus*). *Mathematisch-Naturwissenschaftlichen Fakultät, Rheinischen Friedrich-Wilhelms-Universität*, 189 p.
- Zaher, H., Pol, D., Carvalho, A.B., Riccomini, C., Campos, D.A., Nava, W.R., 2006. Redescription of the cranial morphology of *Mariliasuchus amarali*, and its phylogenetic affinities (Crocodyliformes, Notosuchia). *American Museum Novitates* 3512 (1), 1. [https://doi.org/10.1206/0003-0082\(2006\)3512\[1:rotcmo\]2.0.co;2](https://doi.org/10.1206/0003-0082(2006)3512[1:rotcmo]2.0.co;2).

Appendix A. Supplementary data

Supplementary data to this article can be found online at <https://doi.org/10.1016/j.cretres.2019.104259>.